

Discovery and Preclinical Characterization of 1-Methyl-3-(4-methylpyridin-3-yl)-6-(pyridin-2-ylmethoxy)-1*H*-pyrazolo-[3,4-*b*]pyrazine (PF470): A Highly Potent, Selective, and Efficacious Metabotropic Glutamate Receptor 5 (mGluR5) Negative Allosteric Modulator

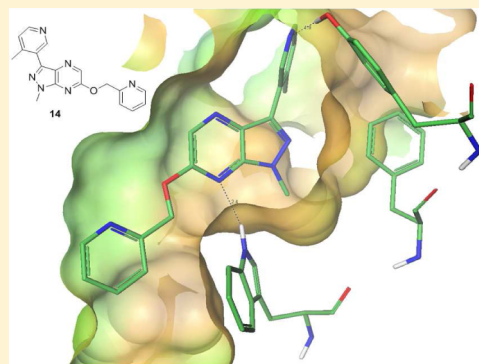
Lei Zhang,^{*,†} Gayatri Balan,^{||} Gabriela Barreiro,[†] Brian P. Boscoe,^{||} Lois K. Chenard,^{||} Julie Cianfrogna,[#] Michelle M. Claffey,^{||} Laigao Chen,[○] Karen J. Coffman,^{||} Susan E. Drozda,^{||} Joshua R. Dunetz,[⊥] Kari R. Fonseca,[‡] Paul Galatsis,[†] Sarah Grimwood,[§] John T. Lazzaro,[⊥] Jessica Y. Mancuso,[∇] Emily L. Miller,[#] Matthew R. Reese,^{||} Bruce N. Rogers,[†] Isao Sakurada,^{||} Marc Skaddan,[○] Deborah L. Smith,[§] Antonia F. Stepan,[†] Patrick Trapa,[‡] Jamison B. Tuttle,[†] Patrick R. Verhoest,[†] Daniel P. Walker,^{||} Ann S. Wright,^{||} Margaret M. Zaleska,[§] Kenneth Zasadny,[○] and Christopher L. Shaffer[‡]

[†]Neuroscience Medicinal Chemistry, [‡]Neuroscience Pharmacokinetics, Dynamics and Metabolism, and [§]Neuroscience Research Unit, Pfizer Inc., Cambridge, Massachusetts 02139, United States

^{||}Neuroscience Medicinal Chemistry, [⊥]Pharmaceutical Sciences, [#]Pharmacokinetics, Dynamics and Metabolism, [∇]Research Statistics, and [○]Bioimaging Center, Pfizer Inc., Groton, Connecticut 06340, United States

S Supporting Information

ABSTRACT: A novel series of pyrazolopyrazines is herein disclosed as mGluR5 negative allosteric modulators (NAMs). Starting from a high-throughput screen (HTS) hit (1), a systematic structure–activity relationship (SAR) study was conducted with a specific focus on balancing pharmacological potency with physicochemical and pharmacokinetic (PK) properties. This effort led to the discovery of 1-methyl-3-(4-methylpyridin-3-yl)-6-(pyridin-2-ylmethoxy)-1*H*-pyrazolo[3,4-*b*]pyrazine (PF470, 14) as a highly potent, selective, and orally bioavailable mGluR5 NAM. Compound 14 demonstrated robust efficacy in a 1-methyl-4-phenyl-1,2,3,6-tetrahydropyridine (MPTP)-rendered Parkinsonian nonhuman primate model of L-DOPA-induced dyskinesia (PD-LID). However, the progression of 14 to the clinic was terminated because of a potentially mechanism-mediated finding consistent with a delayed-type immune-mediated type IV hypersensitivity in a 90-day NHP regulatory toxicology study.



■ INTRODUCTION

Glutamate, the major excitatory neurotransmitter in the brain, exerts its neuromodulatory actions through both ionotropic (e.g., *N*-methyl-D-aspartic acid) and metabotropic glutamate receptors (mGluR). The eight mGluR subtypes (mGluR1–8) are classified into three major groups based on their structure, preferred signal-transduction mechanism, and pharmacology. Group I includes postsynaptically located mGluR1 and mGluR5, which couple to the activation of phospholipase C, leading to the elevation of intracellular calcium and activation of protein kinase C that classically results in an increase in synaptic transmission. Both group II (mGluR2–3) and group III (mGluR4 and mGluR6–8) receptors are located presynaptically and are coupled to the inhibition of adenylate cyclase activity, typically reducing neurotransmitter release.¹ Neurotherapeutic interest in mGluR5 negative allosteric modulators (NAMs) stems from both preclinical and clinical evidence

suggesting their potential for treating anxiety, treatment-resistant depression, addiction, Fragile X Syndrome, and L-DOPA-induced dyskinesia (LID) in Parkinson's disease (PD) patients.² Our work specifically entailed identifying a potent and selective mGluR5 NAM to modulate excessive glutamate release in the basal ganglia to ameliorate PD-LID.³ Several mGluR5 NAMs, including MPEP,⁴ MTEP,⁵ AFQ056,⁶ and ADX48621⁷ (Figure 1), attenuate LID in 1-methyl-4-phenyl-1,2,3,6-tetrahydropyridine (MPTP)-rendered Parkinsonian nonhuman primates (NHP).⁸ For AFQ056 and ADX48621, such findings were also observed in PD-LID patients, providing a proof-of-concept for mGluR5 NAMs in this indication.⁹

Like MPEP and MTEP, mGluR5 NAM clinical candidates¹⁰ (e.g., AFQ056, RG7090,¹¹ and ADX48621) (Figure 1) contain

Received: October 18, 2013

Published: January 6, 2014

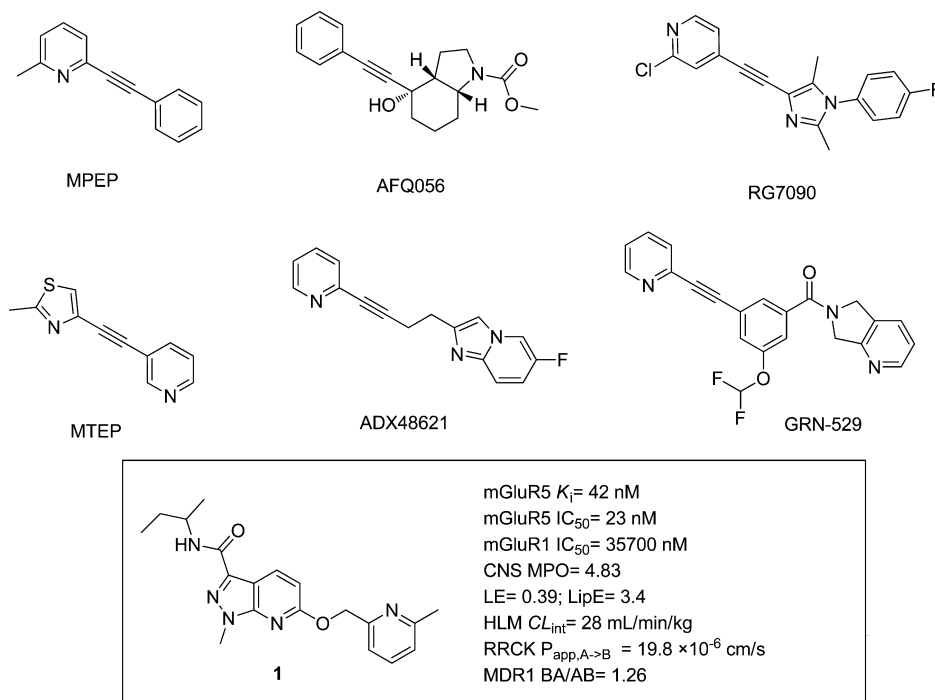


Figure 1. Representative mGluR5 NAMs and alkyne-lacking HTS hit **1**.

an alkyne moiety hypothetically susceptible to metabolic activation that could ultimately cause unacceptable toxicities. This is particularly important for drugs that have daily clinical doses >10 mg.¹² Prior to clinical trials, our group evaluated 4-difluoromethoxy-3-(pyridine-2-ylethynyl)phenyl)-5*H*-pyrrolo[3,4-*b*]pyridine-6(7*H*)-yl methanone (GRN-529),¹³ an alkyne-containing mGluR5 NAM developed by Wyeth researchers, in 8-week rat and NHP regulatory toxicology studies. Although it was safe and well-tolerated in rats (therapeutic index (TI) of 55 at the highest tested dose),¹⁴ biliary epithelial hyperplasia was observed in NHPs at all doses (TI < 4), with increasing severity at increasing doses (Pfizer, unpublished data). Metabolite profiling of NHP hepatic tissue, bile, and plasma samples revealed extensive glutathione conjugation at the alkyne moiety, strongly implicating a structural link to the observed hepatotoxicity. Accordingly, we initiated an effort to identify novel chemotypes lacking an alkyne motif. Described herein is the discovery and optimization of a novel class of pyrazolopyridines derived from a HTS hit (**1**), with a specific focus on balancing potency with physicochemical and pharmacokinetic properties guided by central nervous system multiparameter optimization (CNS MPO),¹⁵ ligand efficiency (LE),¹⁶ and lipophilicity efficiency (LipE).¹⁷ This effort ultimately led to the identification of a highly potent, selective, and orally bioavailable mGluR5 NAM, 1-methyl-3-(4-methylpyridin-3-yl)-6-(pyridin-2-ylmethoxy)-1*H*-pyrazolo[3,4-*b*]pyridine (PF470, **14**), which demonstrated robust efficacy in a MPTP-rendered Parkinsonian NHP model of PD-LID.

RESULTS AND DISCUSSION

Our efforts to identify novel alkyne-lacking mGluR5 NAMs began with a HTS of the internal Pfizer compound file, which yielded a rich collection of chemical matter with 15 structurally distinct chemotypes. Upon further triaging using mGluR5 potency and CNS MPO, a novel pyrazolopyridine amide series, exemplified by **1** (Figure 1), emerged as the most promising

series. Compound **1** demonstrated good mGluR5 binding (K_i of 42 nM) and functional inhibitory activity (IC_{50} of 23 nM) with high functional selectivity over mGluR1 (1543 \times). Further examination of historical HTS data revealed that **1** was inactive in more than 50 other HTS targeting diverse pharmacologies, suggesting its favorable broad-spectrum selectivity. Additionally, **1** possessed favorable physicochemical properties with a high CNS MPO (4.83), reasonable LE (0.39) and LipE (3.4), and many desirable CNS druglike properties,¹⁸ including moderate human liver microsomes-derived intrinsic clearance (HLM CL_{int} = 28 mL/min/kg), high passive transcellular permeability (RRCK $P_{app,A \rightarrow B}$ = 19.8×10^{-6} cm/s),¹⁹ and no human P-glycoprotein (P-gp) liability (MDR1 BA/AB = 1.26).²⁰ Importantly, the modular nature of its chemical structure allowed rapid SAR determination using parallel chemistry. The overall promising properties of **1**, coupled with its chemical tractability, made it an ideal lead for our chemistry efforts.

Initial SAR studies maintained the pyrazolopyridine core while exploring variations on both the head amide group (NR_1R_2) and the ether side chain (R_3) via parallel chemistry (Table 1). A two-point variation library with over 250 analogues was prepared, which allowed rapid insights into the series' general SAR trends. The profiles of representative examples (analogues **2**–**7**) are shown in Table 1. Regarding the amide SAR, primary amines, such as ethylamine (**2**), and amines bearing polar groups (**6** and **7**) generally led to weaker potencies. Simple alkyl or cyclic secondary amines, such as diethyl amine (**3** and **4**) and 2-methyl pyrrolidine (**5**), offered the best potencies and LE, suggesting an interaction of the amide headgroup with a lipophilic binding pocket. For the tail-group SAR, the original HTS side chain, 6-methyl-pyridin-2-yl methyl ether (**2** and **3**), and the corresponding unsubstituted pyridin-2-yl methyl ether (**4**–**7**) were found to be the most preferred, offering comparable potency (**3** vs **4**). However, the less lipophilic pyridine-2-yl methyl ether provided higher LE, LipE, and better HLM stability (<8 vs 42.4 mL/min/kg for **4**

Table 1. mGluR5 Binding (K_i), mGluR5 and mGluR1 Functional Activity (IC_{50}), and Human and Rat Liver Microsomes-Derived Intrinsic Clearance (CL_{int}) of Analogues 2–8

Compound	NR ₁ R ₂	X	R ₃	mGluR5 K_i (nM) ^a	mGluR5 IC_{50} (nM) ^b	LE/LipE ^c	mGluR1 IC_{50} (nM) ^d	HLM CL_{int} (mL/min/kg) ^e	RLM CL_{int} (mL/min/kg) ^f
2		CH		54.6	59.6	0.41/4.1	> 50,000	16.6	982
3		CH		7.80	3.80	0.43/5.4	14,000	42.4	> 1010
4		CH		4.85	5.67	0.46/6.1	5,870	< 8.0	978
5		CH		6.60	14.5	0.43/5.1	29,800	18.2	347
6		CH		114	88.0	0.39/5.6	>50,000	8.2	154
7		CH		899 (n=1)	1002 (n=1)	0.29/2.9	>50,000 (n=1)	ND ^g	ND
8		N		58.0	83.0	0.40/5.7	>50,000	< 8.0	29.7

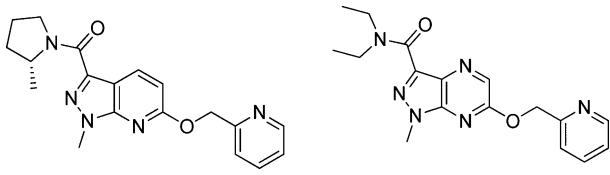
^a K_i (geometric mean, $n \geq 3$ measurements unless specified) in HEK-293FT cells expressing human mGluR5 using [³H]MPEPy ([³H]3-methoxy-5-pyridin-2-ylethynylpyridine). ^b IC_{50} (geometric mean, $n \geq 3$ unless specified) in HEK-293 cells expressing rat mGluR5 using fluorimetric imaging plate reading (FLIPR). ^cLigand efficiency (LE) and lipophilicity efficiency (LipE) calculated using mGluR5 K_i . ^d IC_{50} (geometric mean, $n \geq 3$ unless specified) in HEK-293 cells expressing human mGluR1 using FLIPR. ^eHuman liver microsomes-derived intrinsic clearance. ^fRat liver microsomes-derived intrinsic clearance. ^gND, not determined.

and 3, respectively) and therefore was extensively retained in subsequent SAR studies. A significant species difference in microsomal stability was noted for these pyrazolopyridine analogues; although low-to-moderate HLM CL_{int} could be achieved within the series, rat liver microsomes (RLM)-derived CL_{int} was universally high (>100 mL/min/kg).

Compound 5, an early lead from the initial library, was further profiled in additional in vitro and in vivo PK assays. As shown in Table 1, 5 maintained the mGluR1 selectivity of 1 while significantly improving LE and LipE and lowering HLM CL_{int} but its RLM CL_{int} remained high (347 mL/min/kg). Similar to 1, 5 also had high passive permeability (RRCK $P_{app,A \rightarrow B} = 21 \times 10^{-6}$ cm/s) and no P-gp liability (MDR1 BA/AB = 1.18), which resulted in a rat unbound brain compound concentration-to-unbound plasma compound concentration ratio ($C_{b,u}:C_{p,u}$) of 1.01 (Table 2). However, upon further PK profiling, 5 was found to be labile in rat plasma ($t_{1/2}$ of 5 h) because of amide hydrolysis, but this instability was not observed in human plasma. This rat plasma instability together

with its high RLM CL_{int} resulted in essentially no rat oral bioavailability (F , 0.4%), which precluded 5 and related compounds from advancing further to rat safety studies.

To address the poor rat F of the pyrazolopyridine amide series, we took a two-pronged approach: (A) lower lipophilicity to improve RLM stability and (B) replace the amide with appropriate bioisosteres to improve rat plasma stability. For strategy A, considering that the polarity was generally not tolerated in the amide side chains, more polar central cores were incorporated to reduce lipophilicity, which led to the identification of an alternative pyrazolopyridine core that resolved the oral bioavailability issue. For example, pyrazolopyridine 8 (Table 1) had significantly improved RLM CL_{int} (29.7 mL/min/kg) compared to its corresponding pyrazolopyridine analogue, 4 (978 mL/min/kg), while maintaining comparable LE and LipE despite a drop in mGluR5 potencies. Similar to 5, 8 had very high passive permeability, no susceptibility to P-gp-mediated efflux, and a rat $C_{b,u}:C_{p,u}$ of 0.51 (Table 2). Serendipitously, no detectable hydrolysis of 8

Table 2. Select in Vitro and Rat in Vivo Pharmacokinetic Properties of 5 and 8


PK Properties	5	8
RRCK $P_{app,A \rightarrow B}$ ($\times 10^{-6}$ cm/s) ^a	21.0	31.5
MDR1 BA/AB ^b	1.18	1.00
$f_{u,b}$ (rat) ^c	0.043	0.23
$f_{u,p}$ (rat) ^d	0.066	0.39
$C_{b,u}:C_{p,u}$ ^e	1.01	0.51
$t_{1/2_rat}$ plasma (h) ^f	5	>24
F (%) ^g	0.4%	35%

^aRRCK cells with low transporter activity were isolated from Mardin-Darby canine kidney cells and were used to estimate passive permeability. ^bRatio from the MS-based quantification of $P_{app,A \rightarrow B}$ and $P_{app,B \rightarrow A}$ of the test compound (1 μ M) across contiguous monolayers from MDR1-transfected MDCK cells. ^cUnbound fraction of compound in rat brain homogenate. ^dUnbound fraction of compound in rat plasma. ^e $AUC_{0-T_{last}}$ -derived ratio of unbound brain compound concentration-to-unbound plasma compound concentration in rats (1 mg/kg, sc). ^fThe mean half-life ($t_{1/2}$) of the test compound (1 μ M) following incubation in rat plasma at 37 °C ($n = 3$). ^gBioavailability was calculated from the mean observed $AUC_{0-\infty}$ following single doses of 1 mg/kg iv and 5 mg/kg po ($n = 3$ /dose).

was observed in rat plasma ($t_{1/2} > 24$ h). Most importantly, the combination of lower RLM CL_{int} and rat plasma stability of **8** resulted in much improved rat F (35%).

Concurrent with strategy A, we pursued suitable bioisostere replacements of the metabolically labile amide to address the plasma instability of the pyrazolopyridine amides. As outlined in Table 3, the amide of **5** could be replaced by a phenyl group without significant loss of activity (**9**). Not surprisingly, the overall properties of **9**, particularly around clearance and passive permeability, were suboptimal because of its increased lipophilicity. Nevertheless, it served as a significant SAR inflection point, demonstrating that aryls or heteroaryls were viable amide bioisosteres. Modulating physicochemical properties by incorporating pyridyl to the headgroup (**10** and **11**) considerably improved LipE and increased passive permeability, but did not lower HLM CL_{int} . Prompted by the learnings from strategy A, we incorporated the pyrazolopyridine core into this structural series (analogues **12–21**). Data for the initial analogue (**12**) were mixed. On a positive note, we were pleasantly surprised to see that this core switch, unlike the observation from the amide series, did not result in any loss of mGluR5 activity (**12** vs **11**). However, HLM CL_{int} remained high (94 vs 156 mL/min/kg for **12** and **11**, respectively). Notably, introduction of an *ortho*-methyl group caused a 5-fold decrease in HLM CL_{int} (**13** and **14** vs **12**) while maintaining comparable mGluR5 potency and LipE (**13** vs **10** and **14** vs **12**). We reasoned that this benefit on metabolism might arise from the conformational changes implicated by the *ortho*-substituents, which forced the terminal heteroaryls out of the plane to minimize the unfavorable steric interaction.²¹ Encouraged by this result, we expanded SAR to various heteroaryls bearing *ortho*-substituents. Although many heteroaryls were tolerated, 3-pyridyl, as exemplified by **14**, **15**, and **17**, was optimal for potency. The corresponding 2-pyridyl

analogues (**13** and **16**) were slightly less active, and more significant potency losses were observed with other 5- and 6-membered heteroaryls such as methyl pyridazine (**18**) and pyrazole (**19**). As for the heteroaryl substitutions, small alkyls (**13** and **14**), haloalkyls (**15**), haloalkoxys (**16**), and halogens (**17**) offered the best balance of properties, as evidenced by their mGluR5 potencies and high LE and LipE scores. Bulkier substituents typically did not provide any benefit in potency but rather showed deteriorated overall properties. Further investigation around the *N*-alkyl substitution at the central pyrazole ring revealed that methyl was optimal. Larger side chains, such as ethyl (**20**) or cyclopropyl (**21**), led to lower LE and LipE and elevated HLM CL_{int} .

From these SAR studies, 1-methyl-3-(4-methylpyridin-3-yl)-6-(pyridin-2-ylmethoxy)-1*H*-pyrazolo[3,4-*b*]pyridazine (**14**) was selected for expanded profiling (Figure 2). Compared to the original HTS hit **1**, **14** demonstrated significant multifaceted improvements: it had an almost 50-fold increase in mGluR5 K_i (0.9 vs 42 nM), it further increased mGluR1 functional selectivity to >12000-fold, and it showed no apparent functional agonism (orthosteric or allosteric) or antagonism activities at any other mGluR up to 50 μ M. Broader selectivity screening with **14** revealed no significant activities in kinase panels (<50% inhibition at 10 μ M),²² a proprietary phosphodiesterase (PDE) panel ($IC_{50} > 10$ μ M),²³ and a broad spectrum BioPrint panel²⁴ in which the adenosine A_{2A} receptor had the highest affinity ($K_i = 6.1$ μ M). Importantly, its high potency and selectivity were achieved without compromising overall physicochemical properties: **14** has a highest possible CNS MPO score of 6 and is in compliance with the rule of five²⁵ and the 3/75 analysis (ClogP = 1.5, TPSA = 79 Å^2).²⁶ A good balance of potency and physicochemical properties is reflected by its high LE and LipE (0.49 and 6.3, respectively). These physicochemical properties translated into favorable in vitro PK properties (Table 3), including low-to-moderate HLM CL_{int} (23.7 mL/min/kg), high passive permeability (21 $\times 10^{-6}$ cm/s), and no P-gp liability (MDR1 BA/AB = 1.11).

Intrigued by its exquisite mGluR5 potency and distinct structure from other known alkyne-containing mGluR5 NAMs, we were keen to understand how **14** is bound to the mGluR5 receptor. Although an X-ray crystal structure is unavailable, we were able to gain a preliminary understanding of its binding mode utilizing an mGluR5 homology model refined by mutagenesis experiments.²⁷ Figure 3 shows a superimposition of **14** (green) and MPEP (magenta) docked to this mGluR5 homology model that depicts interactions with key residues. In general, **14** and MPEP appear to occupy the same binding pocket within mGluR5 but show clear distinctions in their binding modes. MPEP forms a hydrogen-bond interaction with residue Y791, and the benzylic ring is sandwiched between residues W784 and F787. The pyridine ring of MPEP also makes an edge-to-face $\pi-\pi$ interaction with residue Y791. Analogous to MPEP, **14** makes a similar hydrogen bond with Y791. However, it also forms a hydrogen-bond interaction with W784 via the central core. This proposed binding mode provides a plausible explanation for the essential role of *ortho*-methyl substitution for potency. As shown in Figure 3, the *ortho*-methyl group torques the pyridyl headgroup orthogonal to the center core and positions it optimally for a hydrogen bond with Y791 while nestling itself in a hydrophobic pocket made by residues F787, L652, and V811 (the last two residues are not shown for clarity).

Table 3. SAR of Aryls and Heteroaryls as Amide Replacements

Compound	Ar	R	X	mGluR5 K_i (nM) ^a	mGluR5 IC_{50} (nM) ^b	LE/LipE ^c	HLM CL_{int} (mL/min/ kg) ^d	RRCK $P_{app,A \rightarrow B}$ ($\times 10^{-6}$ cm/s) ^e	MDR1 BA/AB ^f
9		Me	CH	11.0	105.6	0.45/4.7	122	0.78	0.84
10		Me	CH	5.0	19.6	0.47/5.9	215	11.66	1.18
11		Me	CH	6.2	12.4	0.49/6.3	156	24.4	1.13
12		Me	N	2.3	6.5	0.49/6.6	94	22.5	1.98
13		Me	N	11.0	26.4	0.43/5.6	20	28.5	1.46
14		Me	N	0.9	2.5	0.49/6.3	23.7	22	1.11
15		Me	N	2.8	4.8	0.41/5.4	< 8	21.4	1.28
16		Me	N	6.5	10.7	0.38/5.5	10.5	28.7	1.48
17		Me	N	1.3	10.5	0.47/6.0	33	14.1	2.37
18		Me	N	26.0	25.0	0.41/5.8	< 8	21.5	1.40
19		Me	N	8.1	14.3	0.44/6.1	172	14.4	0.87
20		Et	N	7.0	2.1	0.43/5.7	97	13.8	1.29
21		cyclopropyl	N	10.0	8.0	0.40/5.4	114	19.6	1.39

^a K_i (geometric mean, $n \geq 3$ unless specified) in HEK-293FT cells expressing human mGluR5 using [³H]MPEPy ([³H]3-methoxy-5-pyridin-2-ylethynylpyridine). ^b IC_{50} (geometric mean, $n \geq 3$ unless specified) in HEK-293 cells expressing rat mGluR5 using fluorimetric imaging plate reading (FLIPR). ^cLigand efficiency (LE) and lipophilicity efficiency (LipE) calculated using mGluR5 K_i . ^dHuman liver microsomes-derived intrinsic clearance. ^eRRCK cells with low transporter activity were isolated from Mardin-Darby canine kidney cells and were used to estimate passive permeability. ^fRatio from the MS-based quantification of $P_{app,A \rightarrow B}$ and $P_{app,B \rightarrow A}$ of the test compound (1 μ M) across contiguous monolayers from MDR1-transfected MDCK cells.

In vitro Pharmacology		Selectivity		Physicochemical Properties	
mGluR5 K_i / IC ₅₀ :	0.9 nM / 2.5 nM	Kinase panels:	< 50% inhibition@ 10 μ M	CNS MPO:	6
mGluR1 IC ₅₀ :	30500 nM	PDE panel:	IC ₅₀ > 10 μ M at all PDEs	ClogP / TPSA:	1.5 / 79 \AA
All other mGluRs:	> 50000 nM	Bioprint:	A _{2A} K_i = 6.1 μ M	LE / LipE:	0.49/ 6.30

Figure 2. Potency, selectivity, and physicochemical properties of 14.

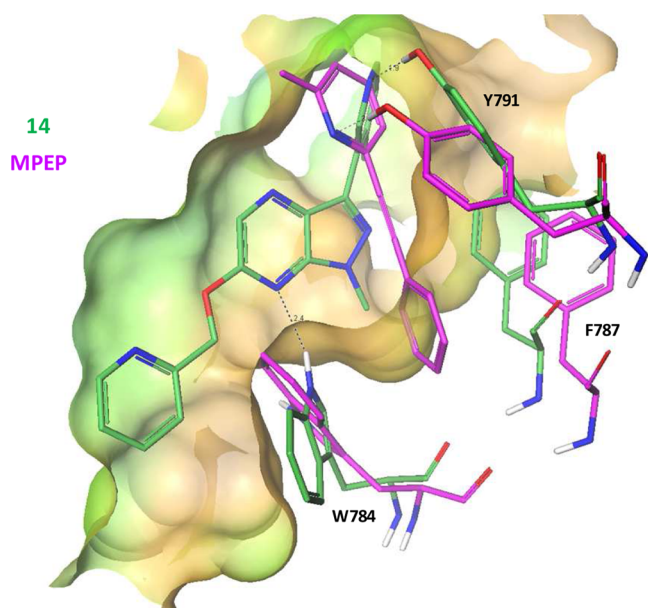


Figure 3. Superimposition of 14 (green) and MPEP (magenta) docked to the mGluR5 homology model depicting interactions with key residues. On the basis of the presented putative binding mode obtained by docking, 14 makes hydrogen bonds to residues W784 and Y791, and the pyridine *ortho*-methyl resides in a hydrophobic pocket made by residues F787, L652, and V811 (not shown). MPEP shows a hydrogen bond with residue Y791, and the benzyl ring is sandwiched between residues W784 and F787. The MPEP pyridine also makes an edge-to-face π - π interaction with residue Y791.

The favorable potency, selectivity, and in vitro PK profile of 14 warranted its PK evaluation in rats and NHP (Table 4). The neuropharmacokinetics of 14 were determined in rats, where it demonstrated net interneurocompartmental equilibrium and parallel elimination rates in both central and peripheral compartments. In rats and NHP, 14 had moderate systemic blood clearance (CL_b) and a low-steady-state volume of distribution (V_{ss}), which resulted in a relatively short half-life ($t_{1/2}$). Acceptable oral bioavailability (F) was achieved in both species.

We next examined the exposure–receptor occupancy (RO) relationship of 14 in rats using an in vivo binding assay and in NHP via positron emission tomography (PET). Rat in vivo RO (IVRO) was determined using a modified [³H]3-methoxy-5-pyridin-2-ylethynylpyridine ([³H]MPEPy) binding protocol.²⁸ The unbound plasma concentration of 14 ($C_{p,u}$) versus mGlu5 RO is shown in Figure 4A. Using a direct-response model, the rat $C_{p,u}$ -derived IC₅₀ (95% confidence interval) for 14 was 1.04 (0.94, 1.15) nM, consistent with its human mGluR5 K_i (0.9 nM).²⁹ For determining RO in NHP ($n = 2$ /dose, crossover design), PET scans were taken using the mGluR5-selective PET ligand [¹⁸F]FPPEB with a vehicle (baseline scan) and four

Table 4. Rat and Monkey PK Properties of 14

property	rat	monkey
$f_{u,b}$ ^a	0.091	ND ⁱ
$f_{u,p}$ ^b	0.097	0.064
$C_{b,u} \cdot C_{p,u}$ ^c	2.0	ND
CL_b (mL/min/kg) ^d	52	18
V_{ss} (L/kg) ^e	1.3	0.69
$t_{1/2}$ (h) ^f	0.31	1.4
F (%)	28 ^g	67 ^h

^aUnbound fraction of compound in brain homogenate. ^bUnbound fraction of compound in plasma. ^cAUC_{0–4}-derived ratio of unbound brain compound concentration-to-unbound plasma concentration determined from rat neuropharmacokinetics study (1 mg/kg, sc; $n = 2$ /time point). ^dObserved blood clearance (CL_b) following a single iv bolus (1 mg/kg, $n = 2$ /species). ^eSteady-state volume of distribution. ^fHalf-life. ^gBioavailability was calculated from the mean observed AUC_{0–∞} following single doses of 1 mg/kg iv ($n = 2$ /dose) and 5 mg/kg po ($n = 3$ /dose). ^hBioavailability was calculated from the mean observed AUC_{0–∞} following single doses of 1 mg/kg iv and 30 mg/kg po ($n = 2$ /dose); ⁱND, not determined.

iv infusion regimens of 14 (displacement scans) to maintain pseudo-steady-state $C_{p,u}$ over the 120 min scanning period targeting mGlu5 RO of ~30, 50, 80, and 90%. An example of a NHP PET displacement image following a dosing regimen targeting 80% RO is shown in Figure 4C.³⁰ Collectively, in the NHP PET studies, 14 had a $C_{p,u}$ -based IC₅₀ of 0.43 (0.30, 0.60) nM³¹ (Figure 4B), which closely paralleled both the human mGluR5 K_i (0.9 nM) and the rat IVRO $C_{p,u}$ -determined IC₅₀ (1.04 nM). The essentially identical human in vitro K_i , rat IVRO $C_{p,u}$ -derived IC₅₀, and NHP PET $C_{p,u}$ -based IC₅₀ provided high confidence in the interspecies translatability of our in vitro screening assay.

Grounded in these well-defined exposure–RO–response correlations, we next wanted to establish a preclinical exposure–RO–response relationship for 14 for PD-LID. Thus, 14 was evaluated in MPTP-rendered Parkinsonian NHP receiving L-DOPA-benserazide with well-characterized consistent and reproducible dyskinesia; this preclinical model³² has shown clinical translatability in PD-LID for the mGluR5 NAMs AFQ056^{8b,9a} and ADX48621.^{8c,9b} This study was a within-subject ($n = 12$), animal-handler-blinded design with treatments pseudo-randomized in a Williams' design including both vehicle and positive control (amantadine, 20 mg/kg, po) arms with ≥ 2 days between treatments based on each compound's $t_{1/2}$ in NHP.³³ A battery of behavioral measures was assessed including activity, Parkinsonian disability, and dyskinesia (composed of chorea and dystonia). On the basis of satellite NHP pharmacokinetics data, three doses of 14 (0.1, 0.32, and 1.0 mg/kg, sc) were chosen to target maximal projected mGlu5 RO of 77, 90, and 97%, respectively (Figure 5). Amantadine ($p < 0.01$) and 14 (0.32 and 1.0 mg/kg, $p < 0.01$ and $p < 0.001$, respectively) showed a statistically

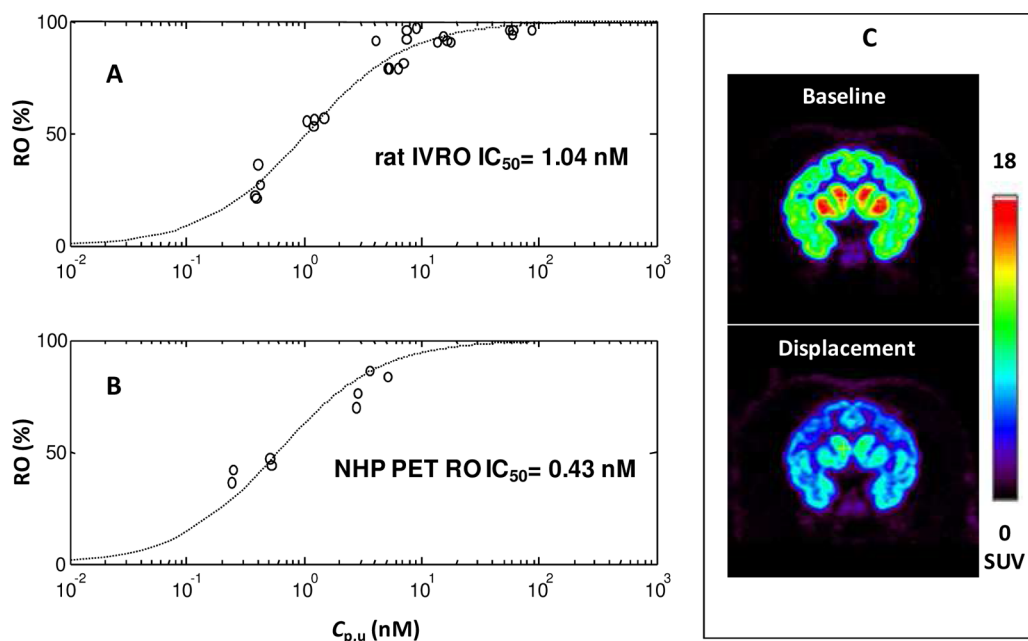


Figure 4. (A, B) mGlu5 RO vs unbound plasma **14** concentration ($C_{p,u}$) in rats and NHP, respectively. C) Coronal views of [18 F]FPPEB-dependent PET images from a NHP receiving vehicle (baseline) and **14** (displacement, 0.0116 mg/kg iv bolus + 0.0180 mg/kg/h infusion over 120 min, 76% RO).

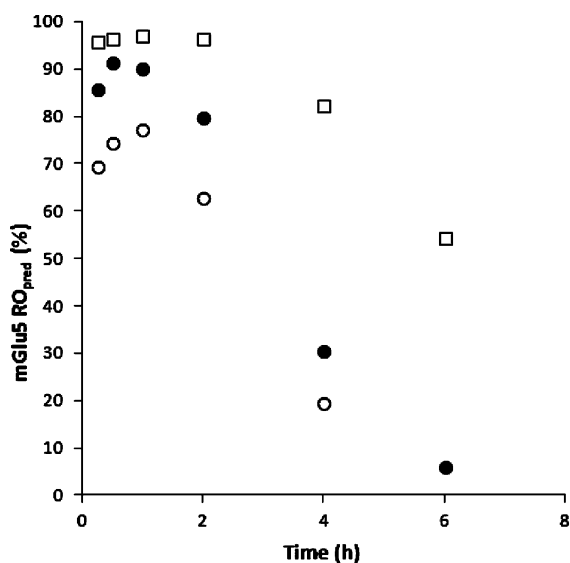


Figure 5. Predicted mGlu5 RO vs time in NHP following 0.1 (○), 0.32 (●), and 1.0 (□) mg/kg, sc, of **14**. At each dose, an RO was calculated by first converting the mean total plasma **14** concentration to $C_{p,u}$ using NHP $f_{u,p}$ (0.064) and compound MW (332.4 ng/nmol) and then incorporating $C_{p,u}$, I_{max} (100%), and IC_{50} (1.04 nM) into the equation $RO = (C_{p,u} I_{max}) / (C_{p,u} + IC_{50})$. Pharmacokinetic samples were collected at 0.25, 0.5, 1, 2, 4, and 6 h postdose ($n = 2$ /dose).

significant reduction in dyskinesia without affecting the L-DOPA-mediated alleviation of Parkinsonism, as measured by the disability score over the 6 h postdose evaluation period (Figure 6). Holistically, these data showed that **14** modulates excessive glutamate release in the basal ganglia and ameliorates LID equivalent to amantadine at mGlu5 RO of $77 < x \leq 90\%$, with even greater attenuation at $>90\%$ RO.

In addition to its robust efficacy in the PD-LID model, **14** also demonstrated sufficient safety and tolerability in 14-day exploratory toxicology studies (ETS) in rats (≤ 80 mg/kg/d,

po) and NHP (≤ 75 mg/kg/d, po) with no significant clinical or histopathological findings observed up to steady-state AUC_{0-24} -based TI of 80 and 30, respectively (the TI denominator is defined as the species-specific total plasma concentration of **14** affording 80% mGlu5 RO over 24 h). On the basis of this holistically favorable data set, **14** underwent 90-day regulatory toxicology studies in rats (≤ 100 mg/kg/d, po) and NHP (≤ 150 mg/kg/d, po). In rats, **14** showed no adverse effects at any tested dose (steady-state TI of 187 at 80 mg/kg/d, po) during the study period. In NHP after 9 days of dosing, erythematous skin lesions presented clinically in multiple body regions in both the high- ($n = 4/4$, 150 mg/kg/day, TI of 460) and mid- ($n = 1/3$, 50 mg/kg/day, TI of 150) dose males, which terminated dosing in the high-dose male group. The timing of clinical symptom onset coupled with the thorough histopathological examination and histological immunostaining features of multiple skin samples taken from all NHP after 90 days of dosing indicated a drug-dependent delayed-type immune-mediated type IV hypersensitivity in these macaques.³⁴

This histopathology was detected in all dose groups, irrespective of the clinical presentation of rash, affording a TI < 10 . Thus, the preclinical development of **14** was terminated. Significantly, in a subsequent 14-day NHP ETS ($n = 1$ /gender/dose) with an mGlu5 NAM structurally distinct from **14** and innocuous in a 14-day rat ETS (TI of 448 at the highest dose tested), the identical NHP-specific microscopic findings were observed in the mid-dose female (TI of 86).²⁹ Collectively, these data suggest this toxicity is potentially mechanism-, not chemotype-, mediated. It is important to note that this specific toxicity could be readily missed without performing a thorough whole-body skin examination (both gross and histopathological), as was the case with **14** in its 14-day NHP ETS because the lack of visible skin rash masked the need for the microscopic evaluation of skin samples, which are typically not collected in exploratory toxicology studies. Thus, neither **14** or any other mGlu5 NAM has been progressed by Pfizer Inc. to clinical trials.

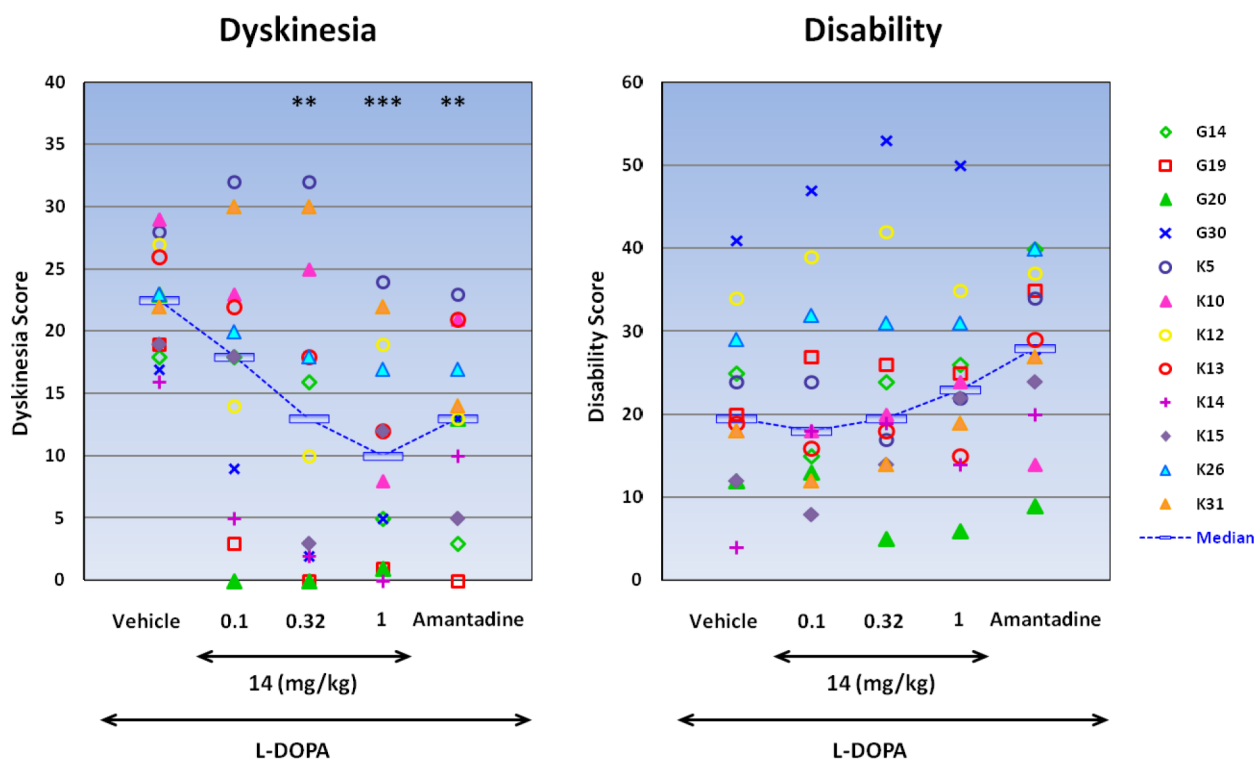
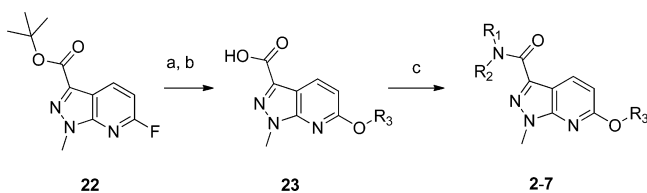


Figure 6. Effect of 14 (0.1, 0.32, and 1.0 mg/kg, sc) and amantadine (20 mg/kg, po) on the dyskinesia and total disability induced by L-DOPA administration to MPTP-rendered Parkinsonian NHP. All groups were first analyzed with a Friedman test followed by Dunn's multiple comparison test; ** $p < 0.01$ and *** $p < 0.001$, cf. vehicle + L-DOPA; $n = 12$ per treatment group. Individual animal scores as well as the median scores are shown.

CHEMISTRY

As illustrated in Scheme 1, analogues 2–7 (Table 1) were synthesized from a known pyrazolopyridine intermediate, 22,³⁵

Scheme 1^a



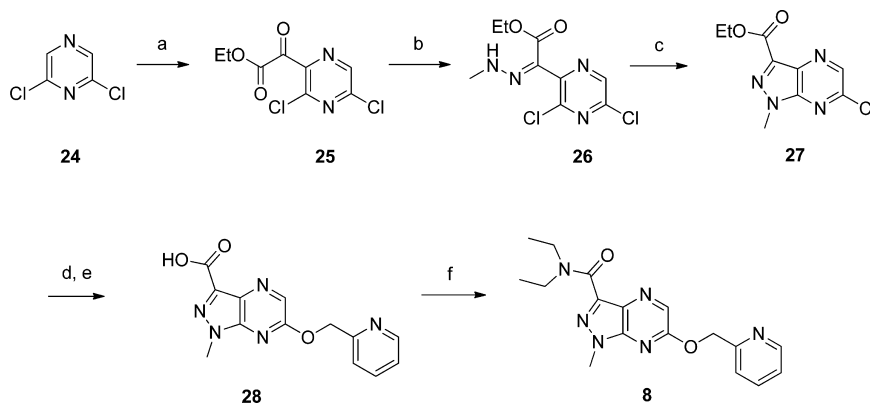
^aReagents and conditions: (a) R_3OH , $KOtBu$, THF, rt; (b) TFA, rt; (c) R_1R_2NH , HBTU, DIPEA, DMF, rt.

via a three-step sequence involving a S_NAr displacement reaction followed by *tert*-butyl ester deprotection and amide formation. These transformations were carried out either in library format to provide variations in both the ether side chains and the amides or in singleton fashion for the library hits follow-up.

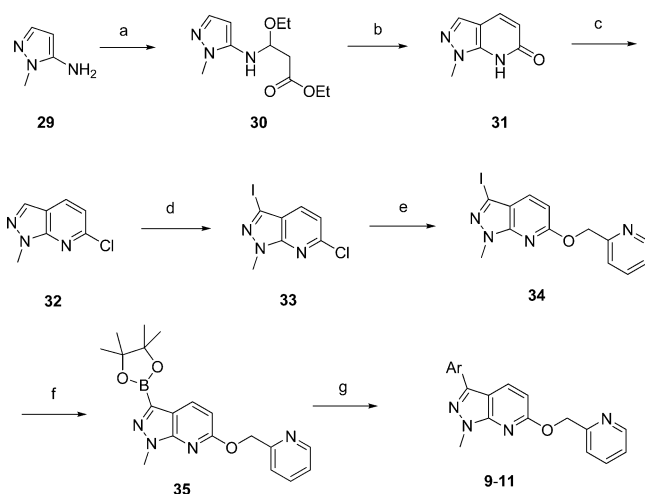
The synthesis of compound 8 is shown in Scheme 2. Starting from dichloropyrazine 24, lithiation followed by trapping with diethyloxalate afforded ketoester 25. Condensation with methyl hydrazine provided hydrazone 26, which, upon treatment with sodium hydride, cyclized to give chloropyrazine ester intermediate 27. Compound 8 was then prepared following a similar three-step sequence as shown in Scheme 1 using pyridin-2-ylmethanol for the S_NAr reaction and diethylamine for the amide formation.

Pyrazolopyridine analogues 9–11 were synthesized in a library format in which an advanced iodo-pyrazolopyridine intermediate, 34, was employed to allow late-stage diversification on the aryl headgroup. As shown in Scheme 3, condensation of aminopyrazole 29 with ethyl propiolate resulted in ester 30, which, upon heating in acetic acid, cyclized to form pyrazolopyridone 31. Subsequent chlorination with phosphorus oxychloride yielded chloropyridine 32, which was further iodinated to give key intermediate 34 with two differentiated halogens as a synthetic handle for further functionalization. For the exemplified analogues 9–11, pyridin-2-ylmethanol was used in a S_NAr reaction to yield intermediate 34, which was converted to boronic ester 35 in situ and subjected to Suzuki coupling to give desired analogues 9–11.

For the SAR study around the pyrazolopyrazine series, a similar synthetic strategy was applied with an analogous chloro-, iodo- pyrazolopyrazine intermediate, 41, targeted as a key intermediate for late-stage diversification (Scheme 4). Starting from the same aminopyrazole, 29, oxidation with sodium nitrite led to a nitroso intermediate 36. The conversion of 36 to pyrazinone 37 was achieved via amine coupling with diethylmalonate followed by cyclization under basic conditions with the nitroso group to form desired pyrazinone 37. Ester hydrolysis gave carboxylic acid 38, which then underwent decarboxylation to afford unsubstituted pyrazinone 39. A similar chlorination and iodination sequence as described in Scheme 3 afforded key intermediate 41. S_NAr displacement with pyridin-2-ylmethanol yielded pyridyl ether 42, which underwent either Negishi coupling with aryl or heteroaryl bromides or Suzuki coupling with aryl or heteroaryl boronic acids to give desired analogues 12–19.

Scheme 2^a

^aReagents and conditions: (a) LiTMP, THF, -78°C , diethyloxalate, 54%; (b) MeNHNH₂, 2 N HCl in Et₂O, EtOH, 80°C ; (c) NaH, THF, 0°C to rt, 71% over two steps; (d) pyridin-2-ylmethanol, KOtBu, THF, rt; (e) 1 N NaOH in H₂O, rt, 93% over two steps; (f) diethylamine, HBTU, DIPEA, DMF, rt, 84%.

Scheme 3^a

^aReagents and conditions: (a) ethyl propiolate, NaOEt, EtOH, 40°C , 90%; (b) AcOH, reflux; (c) POCl₃, 80°C , 78% over two steps; (d) NIS, trifluoroboric acid, CH₃CN, 80°C , 88%; (e) pyridin-2-ylmethanol, KOtBu, THF, rt, 69%; (f) 5,5,5',5'-tetramethyl-2,2'-bi(1,3,2-dioxaborinane), PdCl₂(dppf), KOAc, DMF, 80°C ; (g) ArBr, PdCl₂(dppf), Na₂CO₃, DMF/H₂O (10:1), 80°C .

For analogues bearing different alkyl groups at the central core pyrazole-*N* (20 and 21), an alternative synthetic route was used (Scheme 5). Carbonylation of commercially available bromopyridine 43 led to the formation of ester 44, which, upon condensation with lithiated dichloropyrazine, afforded ketone 45. Subsequent cyclization with alkyl hydrazines yielded chloropyrazines 46a and 46b, which, upon S_NAr displacement with pyridin-2-ylmethanol, afforded desired analogues 20 and 21, respectively.

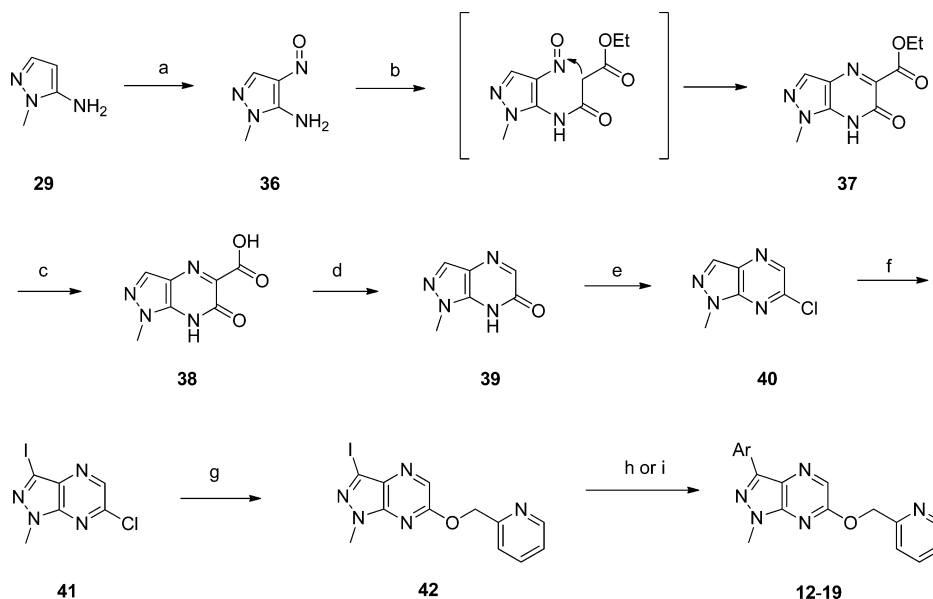
CONCLUSIONS

A novel series of alkyne-lacking pyrazolopyrazines was identified as novel mGluR5 NAMs. The plasma instability and low *F* associated with the original HTS hit were efficiently addressed by focusing SAR efforts on modulating physicochemical properties and replacing the metabolically labile amide with bioisosteres. Compound 14 was identified as the best molecule with a number of desirable attributes, including

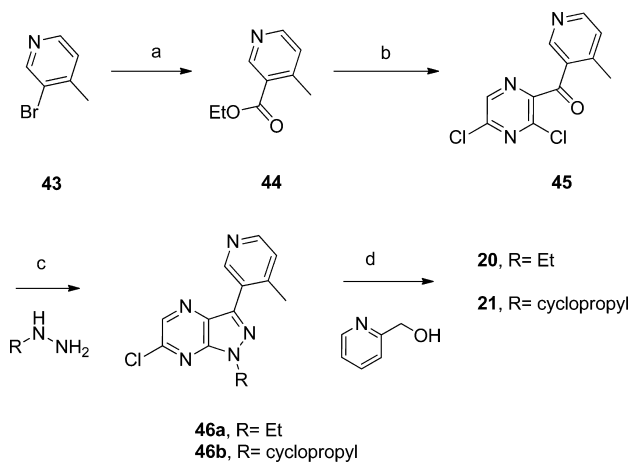
excellent mGluR5 potency and selectivity, favorable PK across species, and a highly reproducible interspecies exposure–RO relationship that could be quantitatively linked to efficacy in a translatable NHP model of PD-L1D. However, the progression of 14 to the clinic was terminated because of findings consistent with a delayed-type immune-mediated type IV hypersensitivity in a 90-day NHP regulatory toxicology study. Importantly, the identical finding was also observed with a structurally distinct mGluR5 NAM, implicating a potential mechanism linkage to this immunotoxicity. Therefore, although there is encouraging efficacy (both preclinically and clinically) reported for mGluR5 NAMs in various indications, further efforts are required to determine definitively whether this NHP delayed-type immune-mediated type IV hypersensitivity is indeed mechanism-based and, consequently, highly relevant to patient safety in ongoing (and future) mGluR5 NAM clinical trials.

EXPERIMENTAL SECTION

Biology. *Recombinant Human mGluR5 Radioligand Binding Assay.* Binding studies were performed in HEK-293FT cells transiently transfected with the human mGluR5. Cells were maintained in 293 FreeStyle Medium (Invitrogen) supplemented with 10 mM HEPES and 50 μg/mL of G418 and transiently transfected using polyethylenimine. After 48 h, cells were centrifuged two times at 3000g for 5 min at 4°C in cold Dulbecco's phosphate-buffered saline. Membrane pellets were then frozen and stored at -80°C until needed. Membrane concentration studies using [³H]MPEPy determined that 0.5–2 mg of frozen cell paste per well was needed, depending on the membrane preparation. A *K_D* of 2 nM for [³H]MPEPy was determined by saturation binding studies. For inhibition binding concentration response studies, compounds were prepared as 30 mM DMSO stocks and were then titrated in 100% DMSO. Membrane paste was thawed, added to cold buffer containing 50 mM Tris with 10 mM EDTA at pH 7.2, homogenized with a polytron, and then centrifuged at 40905g for 10 min at 4°C . The supernatant was discarded, the membrane pellet was resuspended in cold buffer containing 50 mM Tris with 0.1 mM EDTA at pH 7.2, and the suspension was homogenized with a polytron and then spun at 40905g for 10 min at 4°C . The supernatant was discarded, and the membrane pellet was resuspended in cold assay buffer containing 50 mM Tris at pH 7.2, which was homogenized with a polytron. The volume was adjusted to provide 200 μL per well at the desired membrane concentration. A 10× stock solution of [³H]MPEPy in assay buffer was prepared, and the exact concentration was determined by liquid scintillation counting. A final assay concentration of approximately 1 nM was used for inhibition binding experiments.

Scheme 4^a

^aReagents and conditions: (a) NaNO₂, concentrated HCl, 0 °C to rt, 54%; (b) diethylmalonate, NaOEt, EtOH, reflux, 50%; (c) LiOH·H₂O, THF/MeOH/H₂O (6:3:1), rt, 69%; (d) nitrobenzene, reflux, 86%; (e) POCl₃, H₃PO₄, DIPEA, reflux, 67%; (f) NIS, HBF₄, CH₃CN, reflux, 81%; (g) pyridin-2-ylmethanol, KOtBu, THF, 0 °C, 96%; (h) ArBr, *i*PrMgBr/LiCl, THF, rt, then ZnCl₂, 0 °C to rt, then PdCl₂(PPh₃)₂ (20 mol %), 42, 80 °C; (i) 5,5,5',5'-tetramethyl-2,2'-bi(1,3,2-dioxaborinane), PdCl₂(dppf), KOAc, dioxane, 160 °C, 20 min, microwave; ArBr, PdCl₂(dppf), CH₂Cl₂, Cs₂CO₃, dioxane/H₂O (10:1), 65 °C.

Scheme 5^a

^aReagents and conditions: (a) CO, Pd(OAc)₂, 1,1'-bis(diphenylphosphino)ferrocene, Et₃N, EtOH/DMF (2:1), 100 °C, 70%; (b) LiTMP, THF, -80 °C, 82%; (c) RNHNH₂, Et₃N, toluene, rt; (d) pyridin-2-ylmethanol, KOtBu, THF, 0 °C.

Compounds were diluted into assay buffer at 10× final assay concentration in 25 μL per well. Nonspecific binding was determined by the addition of MPEP to control wells at 10× of the final assay concentration of 10 μM. Negative control wells contained equivalent concentrations of DMSO. To each assay well of a 96-well assay plate was added 25 μL of compound or control, 25 μL of [³H]MPEPy stock solution, and 200 μL of membrane stock solution. Plates were incubated at rt for approximately 1 h. Similar results could be obtained by incubation at 4 °C. A filter plate harvester (Packard) was used to transfer well contents to PEI-coated GF/B filter plates (PerkinElmer) that had been prewashed two times with wash buffer containing 50 mM Tris at pH 7.2. After transfer, three washes were performed with wash buffer. Filter plates were allowed to dry overnight before bottom plate seals were applied, 50 μL of Microscint 20 (PerkinElmer) was

added to each well, and clear top plate seals were applied. After a minimum 1 h incubation at rt, filter plates were read on a Trilux (PerkinElmer) with a 1 min read per well. Percent effects of compound inhibition were determined using the DMSO and MPEP control wells. IC₅₀ values were determined with a logistic four-parameter single-site model. K_i values were determined using the Cheng–Prusoff equation and the previously determined K_D. All exemplified active mGluR5 NAMs showed complete inhibition of [³H]MPEPy in their concentration–response curves.

mGluR5 and mGluR1-Mediated Inhibition of Calcium Flux in HEK-293 Cells Expressing Rat mGluR5 or Human mGluR1 Using FLIPR. HEK-293 cells stably expressing rat mGluR5 or human mGluR1 were maintained in Dulbecco's modified Eagle medium with high glucose (DMEM, Gibco) containing 10% fetal bovine serum (HyClone). For FLIPR assays, 15000 cells per well were plated in 30 μL of glutamine-free DMEM (GIBCO) containing 5% FBS and 20 mM HEPES on Matrigel-coated or poly-D-lysine-coated 384-well black-wall clear-bottom polystyrene plates (Greiner). Plates were incubated at 37 °C in 5% CO₂ for 16–24 h. For antagonist evaluation of test compounds, Fluo-8 calcium dye (HD Biosciences) was prepared and added to the cell plates as above. After a 15 min incubation at 37 °C in the dark, dye was removed, and 40 μL of Hank's balanced salt solution containing 1 mM probenecid was added to each well. Five microliters of 9 times the final concentration of test compound was then added to each well using a Bravo (Agilent). Cell plates were then incubated for 15 min at rt in the dark before being placed in a FLIPR Tetra along with compound plates containing glutamate at 5.5 times the final assay concentration. Images were collected before and after the transfer of 10 μL of glutamate per well from the compound plate to the cell plate at rt for a total of 120 images. Excitation and emission wavelengths of 470–495 and 515–575 were used, respectively. The glutamate challenge was adjusted for each assay to produce an approximate EC₇₀ response but was typically between 320 and 1000 nM. The negative control was the glutamate challenge, and the positive control was defined by MPEP (10 μM). Percent effects of compound inhibition were determined using the positive and negative control wells. IC₅₀ values were determined with a logistic four-parameter single-site-fit model.

Rat in Vivo Receptor Occupancy (IVRO) Studies. Male Sprague–Dawley rats (150–200 g; Charles River Laboratories) received **14** (2 mL/kg, sc) and [³H]MPEPy (30 μ Ci/kg, 1 mL/kg, iv) 60 and 1 min, respectively, prior to euthanasia by rapid decapitation. The forebrain (whole brain minus cerebellum) was rapidly dissected and homogenized (3–5 s using a polytron at its highest setting) in 10 volumes of ice-cold assay buffer (10 mM K₂HPO₄ and 100 mM KCl, pH 7.4). Three replicates (400 μ L) of the homogenate were filtered using a vacuum manifold filtration system fitted with 25 mm Whatman GF/B filters soaked in assay buffer. The filters were immediately washed (2 \times 5 mL assay buffer) and transferred to scintillation vials, where they soaked overnight in Ultima Gold (PerkinElmer) before liquid scintillation counting. Total binding was determined by measuring radioactivity in vehicle-treated animals, whereas nonspecific binding was determined using animals treated with a saturating dose of MPEP (50 mg/kg, sc).

Nonhuman Primate (NHP) Positron Emission Tomography (PET) Studies. In NHP (*Macaca fascicularis*, 5 to 6 year old, $n = 2$ /dose, crossover design), PET scans with [¹⁸F]FPEB were taken on multiple days at baseline and with various doses of **14**. In preparation for PET scanning, overnight-fasted NHPs were premedicated with ketamine (10 mg/kg, IM) and glycopyrrolate (0.01 mg/kg, IM), intubated, and maintained under isoflurane anesthesia (1.5–2.0% in oxygen) for the duration of the scan procedure. An iv catheter was placed into the saphenous vein for tracer injection and blood sampling. In addition, an arterial access port was surgically implanted in the femoral artery for assessing a plasma input function for PET data analysis. Dynamic PET scans of 180 min in a Focus 220 microPET scanner (Siemens Medical Systems) with [¹⁸F]FPEB were conducted on the 2 NHPs at both baseline and drug displacement conditions. Each subject underwent five PET scans: baseline and four doses (0.00136, 0.00273, 0.0116, or 0.02589 mg/kg iv bolus plus 0.00212, 0.00424, 0.0180, or 0.0402 mg/kg/h infusion, respectively) of **14** targeting mGlu5 RO of 30, 50, 80, and 90%, respectively. For displacement scans, **14** was administered intravenously as an initial 5 min iv bolus at 30 min prior to [¹⁸F]FPEB injection followed by a constant infusion for 205 min at the designated dose levels to reach a stable total plasma concentration throughout the PET scanning period. [¹⁸F]FPEB was synthesized in high specific activity and radiochemical purity using a Siemens Eclipse cyclotron and a GE FXn radiochemistry module. Before radiotracer injection, an 8 min transmission scan was acquired for attenuation and scatter correction using a ⁵⁷Co point-source. [¹⁸F]FPEB was administered iv as a bolus dose of approximately 1.0 mCi/kg in both baseline and drug-displacement PET scans. For each displacement scan, venous blood samples were collected at three time points (30, 120, and 210 min after the iv bolus of **14**). Whole blood and plasma radioactivity was measured by serial arterial blood sampling, and the percent parent tracer was determined by HPLC. The physiological parameters of each NHP, such as body temperature, respiration, and heart rate, were monitored during the whole compound administration and PET scanning period. PET image data were histogrammed into 25 frames (five 1 min frames, five 5 min frames, and fifteen 10 min frames) over the 180 min dynamic scan duration. Three-dimensional (3D) sinograms were created with corrections for random coincidences and global dead time using a detector span of 3 and maximum ring difference of 47 (the Focus 220 scanner consists of 48 rings of detectors axially). Attenuation and scatter correction maps were created from a measured ⁵⁷Co transmission scan (8 min duration). Images were segmented into four attenuation factors (air, animal bed, water, and bone) with 3D sinogram maps for attenuation and scatter correction created from the segmented transmission image using maximum a posteriori transmission reconstruction (MAP-TR). PET images were reconstructed into a 256 \times 256 \times 95 volume with in-plane pixel dimension of 0.9 mm and slice thickness of 0.8 mm with corrections for detector normalization, decay, attenuation, and scatter using fastMAP (maximum a posteriori) iterative image reconstruction and inverse Fourier rebinning for fully 3D PET.³⁶ Reconstructed images were scaled to standardized uptake values (SUV). Brain regions of interest (ROIs) were defined for each subject on its baseline [¹⁸F]FPEB scan by deformable registration from a segmented NHP

brain atlas. Time-activity curves (TACs) were generated for ROIs such as various cortical regions, putamen, caudate, and cerebellum and fit to a two-tissue (2T) compartment model using PMOD software (PMOD 2.85, PMOD Technologies) for determination of volume of distribution V_t . Receptor occupancy (RO) was determined by analysis of occupancy plots comparing the change in V_t relative to baseline V_t .³⁷ For all displacement scans, the mean total plasma concentration of **14** during the 180 min scanning period was calculated by averaging the exposure measured at 30, 120, and 210 min after the iv bolus of **14**.

Chemistry. General Methods. Solvents and reagents were of reagent grade and were used as supplied by the manufacturer. All reactions were run under a N₂ atmosphere. Organic extracts were routinely dried over anhydrous Na₂SO₄ or MgSO₄. Concentration refers to rotary evaporation under reduced pressure. Chromatography refers to flash chromatography using disposable RediSepR_f 4 to 120 g silica columns or Biotage disposable columns on a CombiFlash Companion or Biotage Horizon automatic purification system. Microwave reactions were carried out in a Smith Creator Personal Chemistry microwave reactor. Purification by mass-triggered HPLC was carried out using Waters XTerra PrepMS C₁₈ columns, 5 μ m, 30 \times 100 mm steel. Compounds were presalted as TFA salts and diluted with 1 mL of dimethyl sulfoxide. Samples were purified by mass-triggered collection using a mobile phase of 0.1% trifluoroacetic acid in water and acetonitrile with a starting gradient of 100% aqueous to 100% acetonitrile over 10 min at a 20 mL/min flow rate. All target compounds were analyzed using ultra-high-performance liquid chromatography/ultraviolet/evaporative light-scattering detection coupled to time-of-flight mass spectrometry (UHPLC/UV/ELSD/TOFMS). Unless otherwise noted, all tested compounds were found to be \geq 95% pure by this method.

UHPLC/MS Analysis. The UHPLC was performed on a Waters ACQUITY UHPLC system (Waters, Milford, MA), which was equipped with a binary solvent-delivery manager, column manager, and sample manager coupled to ELSD and UV detectors (Waters, Milford, MA). Detection was performed on a Waters LCT premier XE mass spectrometer (Waters, Milford, MA). The instrument was fitted with an Acquity BEH (Bridged Ethane Hybrid) C₁₈ column (30 mm \times 2.1 mm, 1.7 μ m particle size, Waters, Milford, MA) operated at 60 $^{\circ}$ C.

Preparations of Analogues 2–7 in Library Format. Step 1: synthesis of intermediate **23**. To a stirred solution of R₃OH (2 equiv) in THF under N₂ at 23 $^{\circ}$ C was added potassium *tert*-butoxide (2 equiv). The reaction mixture was stirred at 23 $^{\circ}$ C for 20 min, and then *tert*-butyl 6-fluoro-1-methyl-1*H*-pyrazolo[3,4-*b*]pyridine-3-carboxylate (**22**) (1 equiv) in THF was added. After 2 h, the reaction mixture was concentrated in vacuo. The resulted thick brown oil was treated with a large excess of trifluoro acetic acid, and the reaction mixture was stirred at 23 $^{\circ}$ C for 18 h. The reaction mixture was concentrated in vacuo and then triturated with methyl *tert*-butyl ether to give carboxylic acid **23** with various side chains (OR₃).

Step 2: amide coupling. Starting amines were obtained preweighed in 2 dram vials (0.08 mmol, 1 equiv). A stock fine suspension containing the trifluoroacetic acid salt of crude template acid (**23**) (1 equiv), DIPEA (8 equiv), and HBTU (1.5 equiv) was prepared in dry *N,N*-dimethylformamide (DMF). To the amines was added 0.5 mL of the above suspension. The vials were capped and shaken at rt for 16 h. Reactions were worked-up by addition of 1.5 mL of 1 N sodium hydroxide solution and 2.5 mL of ethyl acetate. Samples were centrifuged to break up emulsions. Using a Tecan workstation, the organic layers were extracted and loaded onto an SPE cartridge charged with Na₂SO₄ (6 mL, \sim 1 g). The extraction was repeated two times. The combined organics were concentrated in a Genevac. Dry samples were dissolved in 1 mL of dimethyl sulfoxide, filtered, and submitted directly to mass-triggered HPLC purification. The compounds were characterized by UHPLC and MS. For analogues (**3–6**) that were followed-up with resynthesis, their ¹H NMR data are also shown below.

N-Ethyl-1-methyl-6-((6-methylpyridin-2-yl)methoxy)-1*H*-pyrazolo[3,4-*b*]pyridine-3-carboxamide (**2**). The title compound was prepared using (6-methylpyridin-2-yl)methanol and ethyl amine. MS (ES⁺): m/z 326.2 (M + 1). UHPLC: 100% (UV), 100% (ELSD).

N,N-Diethyl-1-methyl-6-((6-methylpyridin-2-yl)methoxy)-1*H*-pyrazolo[3,4-*b*]pyridine-3-carboxamide (3). The title compound was prepared using (6-methylpyridin-2-yl)methanol and diethyl amine (45% yield over two steps in resynthesis). ¹H NMR (400 MHz, DMSO-*d*₆) δ 8.30 (d, *J* = 8.6 Hz, 1 H), 8.18 (t, *J* = 8.2 Hz, 1H), 7.77 (d, *J* = 6.8 Hz, 1H), 7.63 (d, *J* = 7.8 Hz, 1H), 6.89 (d, *J* = 8.6 Hz, 1H), 5.70 (s, 2H), 4.00 (s, 3H), 3.79 (q, *J* = 7.1 Hz, 2H), 3.48 (q, *J* = 7.1 Hz, 2H), 2.68 (s, 3H), 1.18 (dt, *J* = 10.6, 6.9 Hz, 6H). MS (ES⁺): *m/z* 354.2 (M + 1). UHPLC: 100% (UV), 100% (ELSD).

N,N-Diethyl-1-methyl-6-(pyridin-2-ylmethoxy)-1*H*-pyrazolo[3,4-*b*]pyridine-3-carboxamide (4). The title compound was prepared using pyridin-2-yl methanol and diethylamine (71% yield over two steps in resynthesis). ¹H NMR (400 MHz, CD₃OD) δ 8.53 (dt, *J* = 4.9, 0.8 Hz, 1H), 8.25 (d, *J* = 8.8 Hz, 1H), 7.85 (td, *J* = 7.8, 1.7 Hz, 1H), 7.61 (d, *J* = 7.8 Hz, 1H), 7.35 (dd, *J* = 7.5, 5.0 Hz, 1H), 6.83 (d, *J* = 8.6 Hz, 1H), 5.58 (s, 2H), 4.00 (s, 3H), 3.85 (q, *J* = 7.1 Hz, 2H), 3.58 (q, *J* = 6.9 Hz, 2H), 1.27 (q, *J* = 6.7 Hz, 6H). MS (ES⁺): *m/z* 340.1 (M + 1). UHPLC: 100% (UV), 100% (ELSD).

(*R*)-(1-Methyl-6-(pyridin-2-ylmethoxy)-1*H*-pyrazolo[3,4-*b*]pyridin-3-yl)(2-methylpyrrolidin-1-yl)methanone (5). The title compound was prepared using pyridin-2-yl methanol and (*R*)-2-methylpyrrolidine (91% yield over two steps in resynthesis). ¹H NMR as 2:1 mixture of rotamers (400 MHz, DMSO-*d*₆) δ 8.54–8.62 (m, 1H), 8.32–8.41 (m, 1H), 7.83 (td, *J* = 7.7, 2.0 Hz, 1H), 7.56 (d, *J* = 7.8 Hz, 1H), 7.35 (ddd, *J* = 7.6, 4.9, 1.2 Hz, 1H), 6.88 (d, *J* = 8.6 Hz, 1H), 5.56 (s, 2H), 4.94–5.06 (m, 0.35H), 4.23–4.35 (m, 0.7H), 3.97–4.06 (m, 3.7H), 3.86–3.96 (m, 0.7H), 3.53–3.62 (m, 0.7H), 1.91–2.10 (m, 2H), 1.80–1.91 (m, 1H), 1.70 (dd, *J* = 11.3, 5.5 Hz, 1H), 1.51–1.61 (m, 1H), 1.24 (d, *J* = 6.2 Hz, 2H), 1.17 (d, *J* = 6.2 Hz, 1H). MS (ES⁺): *m/z* 352.2 (M + 1). UHPLC: 100% (UV), 100% (ELSD).

(1-Methyl-6-(pyridin-2-ylmethoxy)-1*H*-pyrazolo[3,4-*b*]pyridin-3-yl)(morpholino)methanone (6). The title compound was prepared using pyridin-2-yl methanol and morpholine (64% yield over two steps in resynthesis). ¹H NMR (400 MHz, CDCl₃) δ 8.63 (d, *J* = 4.3 Hz, 1H), 8.35 (d, *J* = 8.6 Hz, 1H), 7.72 (td, *J* = 7.7, 1.8 Hz, 1H), 7.51 (d, *J* = 7.8 Hz, 1H), 7.24 (dd, *J* = 7.1, 5.2 Hz, 1H), 6.84 (d, *J* = 8.8 Hz, 1H), 5.64 (s, 2H), 4.29 (br s, 2H), 4.02 (s, 3H), 3.72–3.90 (m, 6H). *m/z* 354.1 (M + 1). UHPLC: 100% (UV), 100% (ELSD).

1-Methyl-*N*-(3-methylisoxazol-5-yl)methyl-6-(pyridin-2-ylmethoxy)-1*H*-pyrazolo[3,4-*b*]pyridine-3-carboxamide (7). The title compound was prepared in library format using pyridin-2-yl methanol and (3-methylisoxazol-5-yl)methyl amine. MS (ES⁺): *m/z* 379.2 (M + 1). UHPLC: 100% (UV), 99% (ELSD).

Preparation of *N,N*-Diethyl-1-methyl-6-(pyridin-2-ylmethoxy)-1*H*-pyrazolo[3,4-*b*]pyrazine-3-carboxamide (8). Step 1: synthesis of ethyl 2-(3,5-dichloropyrazin-2-yl)-2-oxoacetate (25). To a stirred solution of tetramethyl piperidine (28 mL, 160 mmol) under N₂ at –40 °C was added *n*-BuLi (2.5 M in hexanes, 79 mL, 198 mmol) dropwise. The solution was stirred cold for 20 min. To a cooled (–73 °C, internal thermometer) solution of 2,6-dichloropyrazine (24) (25 g, 160 mmol) and diethyl oxalate (25 g, 170 mmol) in 500 mL of THF under N₂ was added the freshly prepared lithium tetramethyl piperidine solution dropwise so as to maintain the –73 °C internal temperature. The reaction was quenched cold 15 min after the addition was complete by the dropwise addition of acetic acid (9.6 mL, 160 mmol). The reaction mixture was poured into saturated ammonium chloride solution and washed with ethyl acetate (3×). The organic layers were combined, dried over magnesium sulfate, and concentrated in vacuo. The residue was purified using silica gel chromatography with a 0–50% ethyl acetate/heptane gradient as eluent to afford 25 as an orange oil in 54% yield. ¹H NMR (400 MHz, CDCl₃, two rotamers) δ 8.61 (s, 1H), 8.50 (s, 1H), 4.45 (q, *J* = 7.1 Hz, 2H), 4.33 (q, *J* = 7.1 Hz, 2H), 1.41 (t, *J* = 7.2 Hz, 3H), 1.27 (t, *J* = 7.1 Hz, 3H). MS (ES⁺): *m/z* 249.9 (M + 1). GCMS: 100%.

Step 2: synthesis of ethyl 2-(3,5-dichloropyrazin-2-yl)-2-(2-methylhydrazono)acetate (26). To a solution of methyl hydrazine (8.6 mL, 164 mmol) in 90 mL of ethanol at 0 °C was added hydrochloride (2 M in ethyl ether, 82 mL, 164 mmol) dropwise. Ethyl 2-(3,5-dichloropyrazin-2-yl)-2-oxoacetate (25) (38.9 g, 156 mmol) in 90 mL of ethanol was then added dropwise. The reaction mixture was

heated to 80 °C for 2 h. It was then cooled, poured into saturated aqueous NaHCO₃ solution, and washed with ethyl acetate (2×). The organic layers were combined, dried over MgSO₄, and concentrated in vacuo to give 26, which was used without further purification. MS (ES⁺): *m/z* 276.1 (M + 1). GCMS 100%.

Step 3: synthesis of ethyl 6-chloro-1-methyl-1*H*-pyrazolo[3,4-*b*]pyrazine-3-carboxylate (27). To a stirred solution of ethyl 2-(3,5-dichloropyrazin-2-yl)-2-(2-methylhydrazono)acetate (26) from the previous step (theoretical 156 mmol) in 400 mL of THF at 0 °C was added sodium hydride (60% dispersion in mineral oil, 8.75 g, 219 mmol) slowly in portions. The reaction mixture was warmed to 23 °C for 30 min. It was quenched with saturated ammonium chloride solution and then poured into saturated ammonium chloride solution. The pH of the aqueous layer was adjusted to 5 with the addition of 1 N hydrochloride solution, and it was then washed with dichloromethane. The organic layers were combined, dried over MgSO₄, and concentrated in vacuo. The residue was purified using silica gel chromatography with 5% ethyl acetate/dichloromethane as eluent followed by partial concentration from dichloromethane/heptanes to give 27 as an off-white solid in 71% yield. ¹H NMR (400 MHz, CDCl₃) δ 8.74 (s, 1H), 4.59 (q, *J* = 7.0 Hz, 2H), 4.24 (s, 3H), 1.49 (t, *J* = 7.1 Hz, 3H). MS (ES⁺): *m/z* 241.1 (M + 1). UHPLC: 100% (UV), 100% (ELSD).

Step 4: synthesis of 1-methyl-6-(pyridin-2-ylmethoxy)-1*H*-pyrazolo[3,4-*b*]pyrazine-3-carboxylic acid (28). To a stirred solution of potassium *tert*-butoxide (11 g, 94 mmol) in 100 mL of THF under N₂ at 23 °C was added 2-pyridyl carbinol (9.5 mL, 97 mmol). The mixture was stirred at 23 °C for 20 min. The resulting suspension was added by fast drops to ethyl 6-chloro-1-methyl-1*H*-pyrazolo[3,4-*b*]pyrazine-3-carboxylate (27) (15.4 g, 64 mmol) partially dissolved in 200 mL of THF at 0 °C. After the addition was complete in 10 min, 300 mL of 1 N sodium hydroxide solution was added. The reaction mixture was removed from the cold bath and stirred at 23 °C for 2 h. It was then concentrated in vacuo to remove THF and was then chilled in an ice/water bath. The pH was adjusted to 4 by the addition of 200 mL of a 1 N hydrochloride solution. The tan solid that precipitated was collected by vacuum filtration and washed with chilled water to give 16.9 g of 28 in 93% yield over two steps. ¹H NMR (400 MHz, CD₃OD) δ 8.58–8.67 (m, 1H), 8.45 (s, 1H), 8.04 (td, *J* = 7.8, 1.8 Hz, 1H), 7.79 (d, *J* = 7.8 Hz, 1H), 7.53 (ddd, *J* = 7.6, 5.1, 1.2 Hz, 1H), 5.70 (s, 2H), 4.08 (s, 3H). MS (ES⁺): *m/z* 286.1 (M + 1). UHPLC: 85% (UV), 81% (ELSD).

Step 5: synthesis of *N,N*-diethyl-1-methyl-6-(pyridin-2-ylmethoxy)-1*H*-pyrazolo[3,4-*b*]pyrazine-3-carboxamide (8). To a suspension of 1-methyl-6-(pyridin-2-ylmethoxy)-1*H*-pyrazolo[3,4-*b*]pyrazine-3-carboxylic acid (28) (16.9 g, 59 mmol) in 198 mL of DMF at 23 °C was added di-isopropyl ethyl amine (42 mL, 240 mmol), *O*-(benzotriazol-1-yl)-*N,N,N',N'*-tetramethyluronium hexafluorophosphate (25 g, 66 mmol), and diethyl amine (6.9 mL, 65 mmol). The reaction mixture was stirred 1 h at 23 °C. It was then poured into saturated sodium bicarbonate solution and extracted with ethyl acetate (1×) and dichloromethane (2×). The organic layers were combined, washed with a 1 N lithium chloride solution, and then concentrated to approximately half-volume. They were then washed twice with a 1 N hydrochloride solution. The acidic extracts were carefully neutralized to pH 5 with a 6 N sodium hydroxide solution and were then extracted with dichloromethane. These organic extracts were dried over MgSO₄, filtered, and concentrated in vacuo. The crude material was crystallized twice from hot acetonitrile to give 8 in 84% yield. ¹H NMR (400 MHz, CDCl₃) δ 8.65 (d, *J* = 4.1 Hz, 1H), 7.75 (td, *J* = 7.7, 1.8 Hz, 1H), 7.52 (d, *J* = 7.8 Hz, 1H), 7.28 (ddd, *J* = 7.5, 4.9, 1.1 Hz, 1H), 5.63 (s, 2H), 4.04 (s, 3H), 3.65 (q, *J* = 7.2 Hz, 2H), 3.56 (q, *J* = 7.0 Hz, 2H), 1.32 (t, *J* = 7.1 Hz, 3H), 1.21 (t, *J* = 7.0 Hz, 3H). MS (ES⁺): *m/z* 341.2 (M + 1). UHPLC: 89% (UV), 100% (ELSD). The hydrochloride salt of 8 was prepared by dissolving the free base in methanol, adding 2 M hydrochloride in ethyl ether, and concentrating to a slurry. The off-white crystals were collected by vacuum filtration. ¹H NMR (400 MHz, CDCl₃) δ 8.92 (ddd, *J* = 5.9, 1.6, 0.8 Hz, 1H), 8.72 (td, *J* = 7.9, 1.6 Hz, 1H), 8.46 (s, 1H), 8.35 (d, *J* = 8.2 Hz, 1H), 8.12 (t, *J* = 6.9 Hz, 1H), 5.97 (s, 2H), 4.05 (s, 3H), 3.64 (q, *J* = 7.1 Hz, 2H), 3.55 (q, *J* =

7.1 Hz, 2H), 1.30 (t, $J = 7.1$ Hz, 3H), 1.21 (t, $J = 7.0$ Hz, 3H). MS (ES^+): m/z 341.2 ($M + 1$). UHPLC: 100% (UV), 100% (ELSD).

Preparation of 3-Iodo-1-methyl-6-(pyridin-2-ylmethoxy)-1H-pyrazolo[3,4-b]pyridine (34). Step 1: synthesis of ethyl 3-ethoxy-3-((1-methyl-1H-pyrazol-5-yl)amino)propanoate (30). Sodium metal (3.84 g, 166 mmol) was dissolved in ethanol (120 mL) at 40 °C under N_2 . 1-Methyl-1H-pyrazol-5-amine (29) (4.04 g, 41.6 mmol) was then added in one portion. The reaction mixture was stirred for 1 h, and then ethyl propiolate (8.16 g, 83 mmol) was added dropwise over 20 min. Upon completion of addition, the reaction mixture was heated to reflux over 16 h. The reaction was then cooled to rt and concentrated in vacuo. The residue was partitioned between water (200 mL) and ethyl acetate (200 mL). The aqueous layer was further extracted with ethyl acetate (3×100 mL). The organic layers were combined, washed with water and brine, and dried over $MgSO_4$. The solvent was removed in vacuo, and the residue was triturated with petroleum ether to give 9.08 g of 30 as a light brown solid in 90% yield. 1H NMR (400 MHz, $CDCl_3$) δ 8.43 (br s, 1H), 7.37 (d, $J = 1.8$ Hz, 1H), 6.24 (d, $J = 2.0$ Hz, 1H), 4.80 (t, $J = 4.7$ Hz, 1H), 3.72 (m, 2H), 3.69 (s, 3H), 3.57 (m, 2H), 2.73 (d, $J = 4.5$ Hz, 2H), 1.22 (t, $J = 7.0$ Hz, 6H). MS (ES^+): m/z 240.2 ($M - 1$).

Step 2: synthesis of 1-methyl-1H-pyrazolo[3,4-b]pyridin-6(7H)-one (31). 3-Ethoxy-3-((1-methyl-1H-pyrazol-5-yl)amino)propanoate (30) (9.08 g, 37.6 mmol) was dissolved in acetic acid (125 mL) in a round-bottomed flask equipped with a condenser at rt. The reaction mixture was then heated to reflux for 16 h. The reaction was then cooled to rt, and the excess acetic acid was removed in vacuo. The resulting brown solid was further triturated with petroleum ether (2X) and dried in vacuo to give 31 as a light brown solid, which was used in the next step without further purification. 1H NMR (400 MHz, $CDCl_3$) δ 7.72 (d, $J = 9.4$ Hz, 1H), 7.66 (s, 1H), 6.30 (d, $J = 9.2$ Hz, 1H), 3.96 (s, 3H). MS (ES^+): m/z 150.0 ($M + 1$).

Step 3: synthesis of 6-chloro-1-methyl-1H-pyrazolo[3,4-b]pyridine (32). 1-Methyl-1H-pyrazolo[3,4-b]pyridin-6(7H)-one (31) from the previous step was suspended in phosphorus oxychloride (34 mL, 376 mmol), and the reaction mixture was heated at 80 °C under N_2 for 16 h. The reaction mixture was quenched by pouring it into a vigorously stirring mixture of ice water and diethyl ether. After stirring for 40 min, the organic layer was separated, and the aqueous layer was extracted with dichloromethane. The combined organic layers were dried over Na_2SO_4 , filtered, and concentrated. Trituration of the residue with petroleum ether afforded 4.9 g of 32 as a white solid in 78% yield over two steps. 1H NMR (400 MHz, $DMSO-d_6$) δ 7.94 (t, $J = 4.2$ Hz, 2H), 7.08 (d, $J = 8.4$ Hz, 1H), 4.08 (s, 3H). MS (ES^+): m/z 168.1 ($M + 1$).

Step 4: synthesis of 6-chloro-3-iodo-1-methyl-1H-pyrazolo[3,4-b]pyridine (33). To a solution of 6-chloro-1-methyl-1H-pyrazolo[3,4-b]pyridine (32) (4.65 g, 27.7 mmol) in acetonitrile (90 mL) was added *N*-iodosuccinimide (6.44 g, 27.7 mmol) followed by 48% aqueous tetrafluoroboric acid (17.4 mL, 139 mmol). The reaction mixture was heated at 80 °C for 1 h and was then poured into saturated aqueous sodium bicarbonate solution and stirred for 30 min. The resulting precipitate was filtered, and the collected solid was washed with saturated aqueous sodium thiosulfate solution and then with water. Trituration with *n*-pentane provided 7.2 g of 33 as a cream colored solid in 88% yield. 1H NMR (300 MHz, $DMSO-d_6$) δ 7.94 (d, $J = 8.2$ Hz, 1H), 7.27 (d, $J = 8.4$ Hz, 1H), 3.95 (s, 3H). MS (ES^+): m/z 294.0 ($M + 1$).

Step 5: synthesis of 3-iodo-1-methyl-6-(pyridin-2-ylmethoxy)-1H-pyrazolo[3,4-b]pyridine (34). To a stirred solution of pyridin-2-ylmethanol (1.97 mL, 20.4 mmol) in $DMSO$ under N_2 at rt was added potassium *tert*-butoxide (2.3 g, 20.4 mmol). The reaction mixture was stirred for 30 min, and then 6-chloro-3-iodo-1-methyl-1H-pyrazolo[3,4-b]pyridine (33) (5.0 g, 17.0 mmol) was added. The reaction mixture was stirred for additional 20 min, diluted with water (250 mL), and extracted with ethyl acetate (3×150 mL). The combined organic extracts were dried over $MgSO_4$, filtered, and concentrated in vacuo. The residue was purified using silica gel chromatography with a 0–60% ethyl acetate/heptane gradient as eluent to afford 4.33 g of 34 as an off-white solid in 69% yield. 1H NMR (400 MHz, $CDCl_3$) δ 8.58 (d, $J = 4.9$ Hz, 1H), 7.67 (m, 1H), 7.58 (d, $J = 8.6$ Hz, 1H), 7.45 (d, J

= 7.8 Hz, 1H), 7.20 (m, 1H), 6.70 (d, $J = 8.6$ Hz, 1H), 5.57 (s, 2H), 3.95 (s, 3H). MS (ES^+): m/z 366.9 ($M + 1$).

Preparation of Analogues 9–11 in Library Format. Step 1: synthesis of 1-methyl-6-(pyridin-2-ylmethoxy)-3-(4,4,5,5-tetramethyl-1,3,2-dioxaborolan-2-yl)-1H-pyrazolo[3,4-b]pyridine (35). Potassium acetate (1.60 g, 16.4 mmol) was combined with 4,4,4',4',5,5,5',5'-octamethyl-2,2'-bi(1,3,2-dioxaborolane) (1.54 g, 6.0 mmol), 3-iodo-1-methyl-6-(pyridin-2-ylmethoxy)-1H-pyrazolo[3,4-b]pyridine (34) (2.00 g, 5.5 mmol), and [1,1'-bis(diphenylphosphino)ferrocene]-dichloropalladium(II) (117 mg, 0.16 mmol). The mixture was subjected to three cycles of vacuum evacuation followed by filling with nitrogen, and the vial was then charged with degassed DMF (25 mL). After vigorous stirring at rt to provide a homogeneous mixture, the reaction mixture was heated at 80 °C for 1 h, filtered through a plug of Celite, and washed with dichloromethane. The filtrate was concentrated in vacuo to provide corresponding boronic ester 35 as a crude residue, which was used in the following step in library format without further purification. 1H NMR (400 MHz, $CDCl_3$) δ 8.64 (d, $J = 4.1$ Hz, 1H), 7.73 (td, $J = 7.6, 1.7$ Hz, 1H), 7.65 (d, $J = 8.5$ Hz, 1H), 7.51 (d, $J = 7.8$ Hz, 1H), 7.26 (dd, $J = 7.6, 2.7$ Hz, 1H), 6.77 (d, $J = 8.8$ Hz, 1H), 5.63 (s, 2H), 4.02 (s, 3H), 1.28 (s, 6H), 1.26 (s, 6H). MS (ES^+): m/z 367.0 ($M + 1$).

Step 2: library synthesis via Suzuki coupling. Boronic ester residue 35 was combined with sodium carbonate (0.26 mmol), tetrakis-(triphenylphosphine)palladium(0) (0.0016 mmol), and the appropriate aryl or heteroaryl bromide or iodide (0.10 mmol) in DMF (1 mL). The reaction mixture was degassed using two rounds of vacuum evacuation followed by nitrogen fill. The reaction mixture was shaken and heated at 80 °C for 20 h. It was then partitioned between water (1.5 mL) and ethyl acetate (2.5 mL) and vortexed, using centrifugation to break up any emulsions. The organic layer was passed through a solid-phase extraction cartridge filled with Na_2SO_4 (approximately 1 g). This extraction procedure was carried out a total of three times, and the combined filtrates were concentrated and purified via reversed-phase HPLC. The compounds were characterized by UHPLC and MS. For analogues (10 and 11) that were followed-up with resynthesis, their 1H NMR data are also shown below.

1-Methyl-3-phenyl-6-(pyridin-2-ylmethoxy)-1H-pyrazolo[3,4-b]pyridine (9). The title compound was prepared using iodobenzene. MS (ES^+): m/z 317.1 ($M + 1$). UHPLC: 100% (UV), 100% (ELSD).

1-Methyl-3-(pyridin-2-yl)-6-(pyridin-2-ylmethoxy)-1H-pyrazolo[3,4-b]pyridine (10). The title compound was prepared using 2-bromo pyridine (47% yield in resynthesis). 1H NMR (400 MHz, $CDCl_3$) δ 8.75 (d, $J = 8.6$ Hz, 1H), 8.69 (m, 1H), 8.63 (m, 1H), 8.12 (dt, $J = 7.8, 1.0$ Hz, 1H), 7.70–7.76 (m, 2H), 7.53 (d, $J = 7.8$ Hz, 1H), 7.22–7.24 (m, 2H), 6.82 (d, $J = 8.8$ Hz, 1H), 5.65 (s, 2H), 4.07 (s, 3H). MS (ES^+): m/z 318.1 ($M + 1$). UHPLC: 100% (UV), 100% (ELSD).

1-Methyl-6-(pyridin-2-ylmethoxy)-3-(pyridin-3-yl)-1H-pyrazolo[3,4-b]pyridine (11). The title compound was prepared using 3-bromo pyridine (36% yield in resynthesis). 1H NMR (400 MHz, $CDCl_3$) δ 9.17 (br s, 1H), 8.65 (m, 1H), 8.24 (dt, $J = 8.1, 1.8$ Hz, 1H), 8.18 (d, $J = 8.8$ Hz, 1H), 7.74 (td, $J = 7.8, 1.7$ Hz, 1H), 7.54 (d, $J = 7.8$ Hz, 1H), 7.42 (dd, $J = 7.8, 4.8$ Hz, 1H), 7.26 (dd, $J = 8.1, 5.2$ Hz, 1H), 6.83 (d, $J = 8.6$ Hz, 1H), 5.67 (s, 2H), 4.08 (s, 3H). MS (ES^+): m/z 318.1 ($M + 1$). UHPLC: 100% (UV), 100% (ELSD).

Preparation of 3-Iodo-1-methyl-6-(pyridin-2-ylmethoxy)-1H-pyrazolo[3,4-b]pyridine (42). Step 1: synthesis of 1-methyl-4-nitroso-1H-pyrazol-5-amine (36). Concentrated hydrochloric acid (160 mL) was added to a solution of 1-methyl-1H-pyrazol-5-amine (29) (200 g, 2.06 mol) in water (1.4 L), and the mixture was cooled to 0 °C. A solution of sodium nitrite (127.7 g, 1.851 mol) in water (400 mL) was added dropwise while maintaining the temperature below 5 °C, and the reaction was allowed to stir for an additional 2 h at rt. The yellow solid that precipitated during the reaction was isolated via filtration and was washed with cold water to afford 140 g of 36 as a brown solid in 54% yield. This was used in the next step without additional purification. MS (ES^+): m/z 127.1 ($M + 1$). UHPLC: 100% (UV), 100% (ELSD). $R_f = 0.4$ via thin-layer chromatography (TLC) (eluent = 10% methanol in dichloromethane).

Step 2: synthesis of ethyl 1-methyl-6-oxo-6,7-dihydro-1H-pyrazolo[3,4-*b*]pyrazine-5-carboxylate (37). Sodium metal (52.0 g, 2.26 mol) was allowed to react with ethanol (2 L), diethyl malonate (380 mL, 2.50 mol) was added dropwise, and the reaction mixture was stirred for 30 min at rt. 1-Methyl-4-nitroso-1H-pyrazol-5-amine (36) (285 g, 2.26 mol), prepared as described in step 1, was added, and the reaction mixture was heated to reflux for 18 h. Removal of solvent in vacuo provided a residue, which was triturated with petroleum ether and filtered. The resulting solid was dissolved in water, and the pH of the solution was adjusted to a value of 3 to 4 by addition of dilute aqueous hydrochloric acid. The resulting precipitate was isolated via filtration and triturated with *n*-pentane to afford 250 g of 37 as a yellow solid in 50% yield. ¹H NMR (300 MHz, DMSO-*d*₆) δ 8.29 (br s, 1H), 4.35 (q, *J* = 7.1 Hz, 2H), 3.93 (s, 3H), 1.32 (t, *J* = 7.1 Hz, 3H). MS (ES⁺): *m/z* 223.1 (M + 1)

Step 3: synthesis of 1-methyl-6-oxo-6,7-dihydro-1H-pyrazolo[3,4-*b*]pyrazine-5-carboxylic acid (38). Ethyl 1-methyl-6-oxo-6,7-dihydro-1H-pyrazolo[3,4-*b*]pyrazine-5-carboxylate (37) (250 g, 1.12 mol) was partially dissolved in a mixture of THF/methanol/water (6:3:1 ratio, 5.4 L). Lithium hydroxide monohydrate (330 g, 7.86 mol) was added at rt, and the reaction mixture became homogeneous. After the reaction mixture had stirred for 4 h at rt and produced a tan precipitate, the reaction mixture was diluted with ethyl acetate and filtered. The isolated solid was washed with EtOAc and partially dissolved in a minimum quantity of water. After adjustment of the pH to approximately 2 via addition of dilute aqueous hydrochloric acid, the solid was filtered and triturated with *n*-pentane to afford 150 g of 38 as a light brown solid in 69% yield. ¹H NMR (300 MHz, DMSO-*d*₆) δ 8.30 (s, 1H), 3.92 (s, 3H). MS (ES⁺): *m/z* 193.1 (M - 1).

Step 4: synthesis of 1-methyl-1H-pyrazolo[3,4-*b*]pyrazin-6(7H)-one (39). 1-Methyl-6-oxo-6,7-dihydro-1H-pyrazolo[3,4-*b*]pyrazine-5-carboxylic acid (38) (150 g, 0.773 mol) was suspended in nitrobenzene (1.2 L) and heated to reflux for 6 h. After the reaction mixture cooled to rt, it was diluted with petroleum ether and stirred for 30 min; the resulting precipitate was isolated via filtration, and the solid was washed with petroleum ether. Trituration with *n*-pentane provided 100 g of 39 as a brown solid in 86% yield. ¹H NMR (300 MHz, DMSO-*d*₆) δ 12.5 (br s, 1H), 8.12 (s, 1H), 8.01 (s, 1H), 3.90 (s, 3H). MS (ES⁺): *m/z* 149.1 (M - 1).

Step 5: synthesis of 6-chloro-1-methyl-1H-pyrazolo[3,4-*b*]pyrazine (40). 1-Methyl-1,7-dihydro-6H-pyrazolo[3,4-*b*]pyrazin-6-one (39) (100 g, 666 mmol) was suspended in phosphorus oxychloride (306 mL, 3.28 mol). Phosphoric acid (10 mL) was added dropwise over 5 min at rt followed by addition of *N,N*-diisopropylethylamine (116 mL, 666 mmol) dropwise over 30 min. The reaction mixture was heated to reflux for 16 h and was then poured into a vigorously stirring mixture of ice water and diethyl ether. After stirring for 40 min, the organic layer was separated, and the aqueous layer was extracted with dichloromethane. The combined organic layers were dried over Na₂SO₄, filtered, and concentrated. Trituration of the residue with *n*-pentane afforded 75 g of 40 as a light orange solid in 67% yield. ¹H NMR (400 MHz, DMSO-*d*₆) δ 8.72 (s, 1H), 8.52 (s, 1H), 4.06 (s, 3H). MS (ES⁺): *m/z* 169.1 (M + 1).

Step 6: synthesis of 6-chloro-3-iodo-1-methyl-1H-pyrazolo[3,4-*b*]pyrazine (41). To a solution of 6-chloro-1-methyl-1H-pyrazolo[3,4-*b*]pyrazine (40) (50.0 g, 296 mmol) in acetonitrile (500 mL) was added *N*-iodosuccinimide (66.7 g, 296 mmol) followed by 48% aqueous tetrafluoroboric acid (93.2 mL, 713 mmol). The reaction mixture was heated to reflux for 2 h and was then poured into a saturated aqueous sodium bicarbonate solution and stirred for 30 min. The resulting precipitate was filtered; the solid was washed with saturated aqueous sodium thiosulfate solution and then with water. Trituration with *n*-pentane provided 72 g of 41 as a yellow solid in 81% yield. ¹H NMR (300 MHz, DMSO-*d*₆) δ 8.72 (s, 1H), 4.06 (s, 3H). MS (ES⁺): *m/z* 295.0 (M + 1).

Step 7: synthesis of 3-iodo-1-methyl-6-(pyridin-2-ylmethoxy)-1H-pyrazolo[3,4-*b*]pyrazine (42). A solution of potassium *tert*-butoxide (8.38 g, 74.7 mmol) in THF (170 mL) was added dropwise over 20 min to a mixture of 6-chloro-3-iodo-1-methyl-1H-pyrazolo[3,4-*b*]pyrazine (41) (20 g, 68 mmol) and pyridin-2-ylmethanol (7.22 mL,

74.8 mmol) in THF (170 mL) at 0 °C at a rate that maintained the internal reaction temperature below 10 °C. The reaction mixture was stirred for 10 min and was then diluted with water (340 mL) and concentrated in vacuo. The aqueous residue was extracted twice with dichloromethane, and the combined organic extracts were dried over MgSO₄, filtered, and concentrated in vacuo. The residue was triturated with cold ethyl acetate to afford 24.1 g of 42 as a white solid in 96% yield. ¹H NMR (400 MHz, CDCl₃) δ 8.65 (ddd, *J* = 4.9, 1.8, 0.9 Hz, 1H), 8.31 (s, 1H), 7.76 (ddd, *J* = 7.0, 7.6, 1.8 Hz, 1H), 7.52 (br d, *J* = 7.9 Hz, 1H), 7.27–7.31 (m, 1H), 5.63 (s, 2H), 4.05 (s, 3H). MS (ES⁺): *m/z* 367.9 (M + 1).

Preparation of Analogues 12–19 from Advanced Intermediate 42. Method A (Negishi Coupling, Singleton format). A solution of isopropylmagnesium chloride/lithium chloride complex (1.3 M in THF, 2.6 equiv) was added dropwise to a –78 °C solution of the appropriate heteroaryl bromide in THF (2.0 equiv), and the mixture was stirred for 20 min. Zinc chloride (0.5 M solution in THF, 2.6 equiv) was added dropwise; after 10 min, the cooling bath was removed, and the reaction mixture was allowed to stir at rt for 10 min. A mixture of 3-iodo-1-methyl-6-(pyridin-2-ylmethoxy)-1H-pyrazolo[3,4-*b*]pyrazine (42) (1 equiv) and dichlorobis(triphenylphosphine)-palladium(II) (0.2 equiv) was added, and the reaction mixture was immersed in an 80 °C oil bath for 1.5 h. After cooling to rt, the reaction mixture was diluted with ethyl acetate, quenched with a 1 N aqueous sodium hydroxide solution, and then extracted twice with ethyl acetate. The combined organic layers were dried over Na₂SO₄, filtered, and concentrated in vacuo. Two purifications using silica gel chromatography (gradients: 0–6% methanol in dichloromethane followed by 0–3% methanol in dichloromethane) afforded the desired analogues.

Method B (Suzuki Coupling, Library format). Potassium acetate (4 equiv) was dried under vacuum and then combined in a microwave vial with 5,5,5',5'-tetramethyl-2,2'-bi-1,3,2-dioxaborinane (1.7 equiv), 3-iodo-1-methyl-6-(pyridin-2-ylmethoxy)-1H-pyrazolo[3,4-*b*]pyrazine (42) (1.0 equiv), and [1,1'-bis(diphenylphosphino)ferrocene]-dichloropalladium(II) (0.2 equiv). The mixture was subjected to three cycles of vacuum evacuation followed by filling with nitrogen, and the vial was then charged with degassed 1,4-dioxane. After vigorous stirring at rt to provide a homogeneous mixture, the reaction mixture was heated at 160 °C for 35 min under microwave irradiation, filtered through a plug of Celite, and washed with dichloromethane. The filtrate was concentrated in vacuo to provide the corresponding boronic ester as a crude residue, which was used in the following step in library format without further purification. The boronic ester residue from the previous step was combined with cesium fluoride (0.17 mmol), tetrakis(triphenylphosphine)palladium(0) (0.0034 mmol), and the appropriate heteroaryl bromide (0.10 mmol) in 1,4-dioxane (1 mL). The reaction mixture was degassed using two rounds of vacuum evacuation followed by nitrogen fill. The reaction mixture was shaken and heated at 90 °C for 18 h. It was then partitioned between water (1.5 mL) and ethyl acetate (2.5 mL) and vortexed, using centrifugation to break up any emulsions. The organic layer was passed through a solid-phase extraction cartridge filled with Na₂SO₄ (approximately 1 g). This extraction procedure was carried out a total of three times, and the combined filtrates were concentrated and purified via reversed-phase HPLC. The compounds were characterized by UHPLC and MS.

1-Methyl-6-(pyridin-2-ylmethoxy)-3-(pyridin-3-yl)-1H-pyrazolo[3,4-*b*]pyrazine (12). The title compound was prepared using method B (library format) with 3-bromopyridine. MS (ES⁺): *m/z* 319.2 (M + 1). UHPLC: 100% (UV), 100% (ELSD).

1-Methyl-3-(3-methylpyridin-2-yl)-6-(pyridin-2-ylmethoxy)-1H-pyrazolo[3,4-*b*]pyrazine (13). The title compound was prepared using method B (library format, resynthesis) with 2-bromo-3-methylpyridine. ¹H NMR (400 MHz, CDCl₃) δ 8.65 (m, 1H), 8.38 (s, 1H), 7.74 (td, *J* = 7.8, 1.7 Hz, 1H), 7.64 (dd, *J* = 7.8, 1.6 Hz, 1H), 7.52 (d, *J* = 7.8 Hz, 1H), 7.25 (m, 2H), 5.85 (s, 2H), 4.09 (s, 3H), 2.55 (s, 3H). MS (ES⁺): *m/z* 333.2 (M + 1). UHPLC: 100% (UV), 100% (ELSD).

1-Methyl-3-(4-methylpyridin-3-yl)-6-(pyridin-2-ylmethoxy)-1H-pyrazolo[3,4-*b*]pyrazine (14). The title compound was prepared using

method A (Negishi coupling) with 3-bromo-4-methylpyridine. ¹H NMR (400 MHz, DMSO-*d*₆) δ 9.00 (s, 1H), 8.60 (br d, *J* = 4.8 Hz, 1H), 8.49 (d, *J* = 5.0 Hz, 1H), 8.43 (s, 1H), 7.86 (dd, *J* = 7.6, 7.6 Hz, 1H), 7.63 (d, *J* = 7.8 Hz, 1H), 7.35–7.43 (m, 2H), 5.61 (s, 2H), 4.04 (s, 3H), 2.53 (s, 3H). MS (ES⁺): *m/z* 333.1 (M + 1). UHPLC: 100% (UV), 100% (ELSD).

1-Methyl-6-(pyridin-2-ylmethoxy)-3-(4-(trifluoromethyl)pyridin-3-yl)-1H-pyrazolo[3,4-*b*]pyrazine (15). The monofumarate salt of the title compound was prepared using method A (Negishi coupling) with 3-bromo-4-(trifluoromethyl)pyridine followed by treatment with a solution of fumaric acid in a minimal volume of methanol and recrystallization. ¹H NMR (400 MHz, CD₃OD) δ 9.05 (s, 1H), 8.88 (d, *J* = 5.3 Hz, 1H), 8.58 (ddd, *J* = 4.9, 1.7, 0.9 Hz, 1H), 8.33 (s, 1H), 7.87–7.94 (m, 2H), 7.69 (br d, *J* = 7.8 Hz, 1H), 7.39–7.43 (m, 1H), 6.75 (s, 2H), 5.66 (s, 2H), 4.09 (s, 3H). MS (ES⁺): *m/z* 387.1 (M + 1). Anal. Calcd for C₁₈H₁₄F₃N₆O: C, 52.59; H, 3.41; N, 16.73; F, 11.34. Found: C, 52.55; H, 3.10; N, 16.56; F, 11.30.

3-(3-(Difluoromethoxy)pyridin-2-yl)-1-methyl-6-(pyridin-2-ylmethoxy)-1H-pyrazolo[3,4-*b*]pyrazine (16). The title compound was prepared using method A (Negishi coupling) with 2-bromo-3-(difluoromethoxy)pyridine. ¹H NMR (400 MHz, CDCl₃) δ 8.74 (br d, *J* = 4.6 Hz, 1H), 8.66 (br d, *J* = 4.5 Hz, 1H), 8.41 (s, 1H), 7.78 (br dd, *J* = 7.7, 7.6 Hz, 1H), 7.73 (br d, *J* = 8.2 Hz, 1H), 7.55 (br d, *J* = 7.8 Hz, 1H), 7.40 (dd, *J* = 8.3, 4.8 Hz, 1H), 7.30 (br dd, *J* = 7.1, 5.1 Hz, 1H), 6.74 (t, *J*_{HF} = 74.7 Hz, 1H), 5.67 (s, 2H), 4.12 (s, 3H). MS (ES⁺): *m/z* 385.1 (M + 1). UHPLC: 100% (UV), 100% (ELSD).

3-(5-Chloro-4-methylpyridin-3-yl)-1-methyl-6-(pyridin-2-ylmethoxy)-1H-pyrazolo[3,4-*b*]pyrazine (17). The title compound was prepared using method A (Negishi coupling) with 3-bromo-5-chloro-4-methylpyridine. ¹H NMR (400 MHz, CDCl₃) δ 8.87 (s, 1H), 8.68 (br d, *J* = 4.9 Hz, 1H), 8.60 (s, 1H), 8.35 (s, 1H), 7.82 (ddd, *J* = 7.8, 7.6, 1.6 Hz, 1H), 7.59 (br d, *J* = 7.8 Hz, 1H), 7.34 (br dd, *J* = 7.3, 5.2 Hz, 1H), 5.71 (s, 2H), 4.12 (s, 3H), 2.60 (s, 3H). MS (ES⁺): *m/z* 367.1 (M + 1). UHPLC: 100% (UV), 100% (ELSD).

1-Methyl-6-(pyridin-2-ylmethoxy)-3-(4-methyl-pyridazin-3-yl)-1H-pyrazolo[3,4-*b*]pyrazine (18). The title compound was prepared using method A (singleton format) with 3-bromo-4-methyl-pyridazine in 18% yield. ¹H NMR (400 MHz, CDCl₃) δ 9.02 (br d, *J* = 5.1 Hz, 1H), 8.60 (ddd, *J* = 4.6, 1.5, 1.0 Hz, 1H), 8.35 (s, 1H), 7.69 (td, *J* = 7.6, 1.8 Hz, 1H), 7.47 (br d, *J* = 7.8 Hz, 1H), 7.35 (dd, *J* = 5.3, 1.0 Hz, 1H), 7.21 (m, 1H), 5.60 (s, 2H), 4.07 (s, 3H), 2.51 (s, 3H). MS (ES⁺): *m/z* 334.1 (M + 1). UHPLC: 100% (UV), 100% (ELSD).

3-(1,5-Dimethyl-1H-pyrazol-4-yl)-1-methyl-6-(pyridin-2-ylmethoxy)-1H-pyrazolo[3,4-*b*]pyrazine (19). The title compound was prepared using method A (singleton format) with 4-bromo-1,5-dimethyl-1H-pyrazole in 51% yield. ¹H NMR (400 MHz, CDCl₃) δ 8.66 (ddd, *J* = 4.9, 1.6, 0.8 Hz, 1H), 8.29 (s, 1H), 8.22 (br s, 1H), 7.77 (ddd, *J* = 7.8, 7.6, 1.8 Hz, 1H), 7.55 (br d, *J* = 7.8 Hz, 1H), 7.27–7.31 (m, 1H), 5.65 (s, 2H), 4.02 (s, 3H), 3.88 (s, 3H), 2.65 (s, 3H). MS (ES⁺): *m/z* 336.0 (M + 1). UHPLC: 100% (UV), 100% (ELSD).

Preparation of 1-Ethyl-3-(4-methylpyridin-3-yl)-6-(pyridin-2-ylmethoxy)-1H-pyrazolo[3,4-*b*]pyrazine (20). Step 1: synthesis of ethyl 4-methylpyridine-3-carboxylate (**44**). A mixture of 3-bromo-4-methylpyridine (**43**) (160 g, 0.930 mol), 1,1'-bis(diphenylphosphino)-ferrocene (103 g, 0.186 mol), triethylamine (257 mL, 1.84 mol), and palladium(II) acetate (20.8 g, 92.7 mmol) in ethanol (2.4 L) and DMF (1.2 L) was placed in a sealed autoclave and stirred under a carbon monoxide atmosphere (2.5 MPa) at 100 °C for 18 h. The mixture was cooled to rt and concentrated in vacuo to remove ethanol. Solids were removed via filtration, and the filter cake was washed with ethyl acetate (1 L). The combined filtrates were diluted with additional ethyl acetate (1 L) and washed with a saturated aqueous sodium chloride solution (3 × 1 L). The organic layer was dried over Na₂SO₄, filtered, and concentrated in vacuo. The crude products from four runs of this reaction were combined and purified by chromatography on silica gel (gradient: 4–9% ethyl acetate in petroleum ether), affording 430 g of **44** as a colorless oil in 70% yield. ¹H NMR (400 MHz, CDCl₃) δ 9.05 (s, 1H), 8.53 (d, *J* = 5.0 Hz, 1H), 7.15 (d, *J* = 5.0 Hz, 1H), 4.38 (q, *J* = 7.1 Hz, 2H), 2.60 (s, 3H), 1.39 (t, *J* = 7.2 Hz, 3H). GCMS (ES⁺): *m/z* 166.2 (M + 1).

Step 2: synthesis of (3,5-dichloropyrazin-2-yl)(4-methylpyridin-3-yl)methanone (**45**). A solution of 2,2,6,6-tetramethylpiperidine (30 mL, 180 mmol) in THF (1.5 L) was cooled to –40 °C. *n*-Butyl lithium (2.5 M solution, 80 mL, 200 mmol) was slowly added, and the reaction mixture was allowed to warm to 0 °C and stir for 20 min. The reaction mixture was cooled to –80 °C, and a solution of 2,6-dichloropyrazine (25 g, 170 mmol) in tetrahydrofuran (200 mL) was added dropwise. After the reaction mixture had stirred for 1 h at –80 °C, ethyl 4-methylpyridine-3-carboxylate (**44**) (23 g, 140 mmol) was slowly added, and the resulting mixture was stirred at –80 °C for 2 h. The reaction was quenched by slow addition of acetic acid (15 mL), after which it was allowed to warm to rt. The mixture was then diluted with ethyl acetate (1.2 L) and washed sequentially with aqueous hydrochloric acid (0.1 M, 2 × 500 mL), saturated aqueous sodium bicarbonate solution (500 mL), and saturated aqueous sodium chloride solution (500 mL). The organic layer was filtered and concentrated in vacuo. Twenty batches following this protocol were combined to give 620 g of **45** as a brown oil in 82% yield. ¹H NMR (400 MHz, CDCl₃) δ 8.63 (d, *J* = 5.0 Hz, 1H), 8.53 (s, 1H), 7.32 (d, *J* = 5.0 Hz, 1H), 2.63 (s, 3H). MS (ES⁺): *m/z* 268.1 (M + 1).

Step 3: synthesis of 6-chloro-1-ethyl-3-(4-methylpyridin-3-yl)-1H-pyrazolo[3,4-*b*]pyrazine (**46a**). Triethylamine (99%, 0.66 mL, 4.7 mmol) was added to a solution of (3,5-dichloropyrazin-2-yl)(4-methylpyridin-3-yl)methanone (**45**) (208 mg, 0.776 mmol) in toluene (4 mL). After addition of the oxalate salt of ethyl hydrazine (350 mg, 2.33 mmol), the reaction mixture was stirred at rt for 72 h. Water and ethyl acetate were added, and the mixture was filtered through Celite. The aqueous layer was extracted twice with ethyl acetate, and the combined organic layers were dried over MgSO₄, filtered, and concentrated in vacuo. Purification via silica gel chromatography (gradient: 0–100% ethyl acetate in heptane) afforded 65 mg of **46a** as a yellow solid in 32% yield. ¹H NMR (400 MHz, CDCl₃) δ 9.20 (br s, 1H), 8.59 (s, 1H), 8.55 (br d, *J* = 5.2 Hz, 1H), 7.34–7.37 (m, 1H), 4.62 (q, *J* = 7.3 Hz, 2H), 2.64 (br s, 3H), 1.63 (t, *J* = 7.3 Hz, 3H). MS (ES⁺): *m/z* 274.0 (M + 1).

Step 4: synthesis of 1-ethyl-3-(4-methylpyridin-3-yl)-6-(pyridin-2-ylmethoxy)-1H-pyrazolo[3,4-*b*]pyrazine (**20**). The title compound was prepared according to step 7 of the preparation of advanced intermediate **42** using 6-chloro-1-ethyl-3-(4-methylpyridin-3-yl)-1H-pyrazolo[3,4-*b*]pyrazine (**46a**) and pyridin-2-ylmethanol as reactants. ¹H NMR (400 MHz, CDCl₃) δ 9.08 (br s, 1H), 8.66 (ddd, *J* = 4.9, 1.8, 0.9 Hz, 1H), 8.51 (d, *J* = 5.0 Hz, 1H), 8.35 (s, 1H), 7.77 (ddd, *J* = 7.8, 7.6, 1.8 Hz, 1H), 7.53–7.57 (m, 1H), 7.26–7.31 (m, 2H), 5.66 (s, 2H), 4.50 (q, *J* = 7.2 Hz, 2H), 2.59 (s, 3H), 1.56 (t, *J* = 7.3 Hz, 3H). MS (ES⁺): *m/z* 347.1 (M + 1). UHPLC: 100% (UV), 100% (ELSD).

Preparation of 1-Cyclopropyl-3-(4-methylpyridin-3-yl)-6-(pyridin-2-ylmethoxy)-1H-pyrazolo[3,4-*b*]pyrazine (21). Step 1: synthesis of 6-chloro-1-cyclopropyl-3-(4-methylpyridin-3-yl)-1H-pyrazolo[3,4-*b*]pyrazine (**46b**). The title compound was prepared according to step 3 of the preparation of compound **20** using the hydrochloride salt of cyclopropylhydrazine as reactant. ¹H NMR (400 MHz, CDCl₃) δ 9.16 (br s, 1H), 8.59 (s, 1H), 8.54 (d, *J* = 5.2 Hz, 1H), 7.32 (br d, *J* = 5.2 Hz, 1H), 3.97–4.03 (m, 1H), 2.61 (br s, 3H), 1.40–1.46 (m, 2H), 1.22–1.28 (m, 2H). MS (ES⁺): *m/z* 286.0 (M + 1).

Step 2: synthesis of 1-cyclopropyl-3-(4-methylpyridin-3-yl)-6-(pyridin-2-ylmethoxy)-1H-pyrazolo[3,4-*b*]pyrazine (**21**). The title compound was prepared according to step 7 of the preparation of advanced intermediate **42** using 6-chloro-1-cyclopropyl-3-(4-methylpyridin-3-yl)-1H-pyrazolo[3,4-*b*]pyrazine (**46b**) and pyridin-2-ylmethanol as reactants. ¹H NMR (400 MHz, CDCl₃) δ 9.07 (br s, 1H), 8.67 (ddd, *J* = 4.9, 1.8, 0.8 Hz, 1H), 8.50 (d, *J* = 5.1 Hz, 1H), 8.35 (s, 1H), 7.77 (ddd, *J* = 7.8, 7.6, 1.8 Hz, 1H), 7.55–7.59 (m, 1H), 7.26–7.31 (m, 2H), 5.68 (s, 2H), 3.83–3.89 (m, 1H), 2.57 (s, 3H), 1.33–1.38 (m, 2H), 1.13–1.19 (m, 2H). MS (ES⁺): *m/z* 359.1 (M + 1). UHPLC: 100% (UV), 100% (ELSD).

■ ASSOCIATED CONTENT

Supporting Information

NHP PD-LID model protocol and expanded SAR tables with mGluR5 binding and functional activity ranges. This material is available free of charge via the Internet at <http://pubs.acs.org>. PF470 (14), also known as PF-06297470, is now commercially available at Sigma-Aldrich (product no. PZ0219).

■ AUTHOR INFORMATION

Corresponding Author

*Phone: +1 617 395 0640. Fax: +1 860 686 5285. E-mail: Lei.Zhang3@pfizer.com.

Notes

The authors declare no competing financial interest.

■ ACKNOWLEDGMENTS

We thank MOTAC Neuroscience (Beijing, People's Republic of China) for performing the NHP PD-LID study. We also thank the Pfizer ADME technology group for generating the in vitro pharmacokinetic data in support of the SAR effort.

■ ABBREVIATIONS USED

2T, two-tissue; CL_{int} , intrinsic clearance; F , oral bioavailability; FPB, 3-fluoro-5-[(pyridin-3-yl)ethynyl]benzotrile; HLM, human liver microsomes; LipE, lipophilicity efficiency; MPEP, 2-methyl-6-(phenylethynyl)pyridine; MPEPy, 3-methoxy-5-pyridin-2-ylethynylpyridine; MPTP, 1-methyl-4-phenyl-1,2,3,6-tetrahydropyridine; MPO, multiparameter optimization; MTEP, 3-((2-methyl-4-thiazolyl)ethynyl)pyridine; NHP, non-human primate; PDE, phosphodiesterase; PD-LID, L-DOPA-induced dyskinesia in Parkinson's disease; PET, positron emission tomography; RO, receptor occupancy; RLM, rat liver microsomes; RRCK, RR canine kidney; TAC, time-activity curve; TI, therapeutic index; V_{ss} , steady-state volume of distribution; V_d , volume of distribution

■ REFERENCES

- (1) Conn, P. J.; Pin, J.-P. Pharmacology and functions of metabotropic glutamate receptors. *Annu. Rev. Pharmacol. Toxicol.* **1997**, *37*, 205–237.
- (2) Bach, P.; Isaac, M.; Slassi, A. Metabotropic glutamate receptor 5 modulators and their potential therapeutic applications. *Expert Opin. Ther. Pat.* **2007**, *17*, 371–384.
- (3) Mela, F.; Marti, M.; Dekundy, A.; Danysz, W.; Morari, M.; Cenci, M. A. Antagonism of metabotropic glutamate receptor type 5 attenuates L-DOPA-induced dyskinesia and its molecular and neurochemical correlates in a rat model of Parkinson's disease. *J. Neurochem.* **2007**, *101*, 483–497.
- (4) Gasparini, F.; Lingenhöhl, K.; Stoehr, N.; Flor, P. J.; Heinrich, M.; Vranesic, I.; Biollaz, M.; Allgeier, H.; Heckendorn, R.; Urwyler, S.; Varney, M. A.; Johnson, E. C.; Hess, S. D.; Rao, S. P.; Sacaan, A. I.; Santori, E. M.; Velicelebi, G.; Kuhn, R. Methyl-6-(phenylethynyl)-pyridine (MPEP), a potent, selective and systematically active mGluR5 receptor antagonist. *Neuropharmacology* **1999**, *38*, 493–503.
- (5) Cosford, N. D. P.; Tehrani, L.; Roppe, J.; Schweiger, E.; Smith, N. D.; Anderson, J.; Bristow, L.; Brodtkin, J.; Jiang, X.; McDonald, I.; Rao, S.; Washburn, M.; Varney, M. A. 3-[(2-Methyl-1,3-thiazol-4-yl)ethynyl]-pyridine: A potent and highly selective metabotropic glutamate subtype 5 receptor antagonist with anxiolytic activity. *J. Med. Chem.* **2003**, *46*, 204–206.
- (6) The structure of AFQ056 (Mavoglurant) was first disclosed in international nonproprietary names for pharmaceutical substances (INN). *WHO Drug Information*; World Health Organization: Geneva, Switzerland, 2010; Vol. 24, p 381.

(7) The structure of ADX48621 (Dipraglurant) was first disclosed in international nonproprietary names for pharmaceutical substances (INN). *WHO Drug Information*; World Health Organization: Geneva, Switzerland, 2009; Vol. 23, p 328.

(8) (a) Morin, N.; Grégoire, L.; Gomez-Mancilla, B.; Gasparini, F.; Di Paolo, T. Effect of the metabotropic glutamate receptor type 5 antagonists MPEP and MTEP in parkinsonian monkeys. *Neuropharmacology* **2010**, *58*, 981–986. (b) Grégoire, L.; Morin, N.; Ouattara, B.; Gasparini, F.; Bilbe, G.; Johns, D.; Vranesic, I.; Sahasranaman, S.; Gomez-Mancilla, B.; Di Paolo, T. The acute antiparkinsonian and antidyskinetic effect of AFQ056, a novel metabotropic glutamate receptor type 5 antagonist, in L-DOPA-treated parkinsonian monkeys. *Parkinsonism Related Disord.* **2011**, *17*, 270–276. (c) *Addex's ADX48621 effective in preclinical Parkinson's disease studies*; Addex Pharmaceuticals Press Release: Geneva, Switzerland, 2010; <http://www.addextherapeutics.com/investors/press-releases/>.

(9) (a) Berg, D.; Godau, J.; Trenkwalder, C.; Eggert, K.; Csoti, I.; Storch, A.; Huber, H.; Morelli-Canelo, M.; Stamelou, M.; Ries, V.; Wolz, M.; Schnieder, C.; Di Paolo, T.; Gasparini, F.; Hariry, S.; Vandemeulebroecke, M.; Abi-Saab, W.; Cooke, K.; Johns, D.; Gomez-Mancilla, B. AFQ056 treatment of levodopa-induced dyskinesias: results of 2 randomized controlled trials. *Mov. Disord.* **2011**, *26*, 1243–1250. (b) *Addex reports positive top line phase IIa data for dipraglurant in Parkinson's disease levodopa-induced dyskinesia (PD-LID)*. Addex Pharmaceuticals Press Release: Geneva, Switzerland, 2012; <http://www.addextherapeutics.com/investors/press-releases/>.

(10) Emmitte, K. A. mGlu5 negative allosteric modulators: A patent review (2010–2012). *Expert Opin. Ther. Pat.* **2013**, *23*, 393–408.

(11) For RG7090 structure, see: U.S. FDA Orphan Drug Designations and Approvals. http://www.accessdata.fda.gov/scripts/opdlisting/oopd/OOPD_Results_2.cfm?index_Number=333211.

(12) Kalgutkar, A. S.; Gardner, I.; Obach, R. S.; Shaffer, C. L.; Callegari, E.; Henne, K. R.; Mutlib, A. E.; Dalvie, D. K.; Lee, J. S.; Nakai, Y.; O'Donnell, J. P.; Boer, J.; Harriman, S. P. A comprehensive listing of bioactivation pathways of organic functional groups. *Curr. Drug Metab.* **2005**, *6*, 161–225.

(13) (a) Hughes, Z. A.; Neal, S. J.; Smith, D. L.; Rizzo, S. J.; Pulicicchio, C. M.; Lotarski, S.; Lu, S.; Dwyer, J. M.; Brennan, J.; Olsen, M.; Bender, C. N.; Kouranova, E.; Andree, T. H.; Harrison, J. E.; Whiteside, G. T.; Springer, D.; O'Neil, S. V.; Leonard, S.; Schechter, L. E.; Dunlop, J.; Rosenzweig-Lipson, S.; Ring, R. H. Negative allosteric modulation of metabotropic glutamate receptor 5 results in broad spectrum activity relevant to treatment resistant depression. *Neuropharmacology* **2013**, *66*, 202–214. (b) Sperry, J. B.; Farr, R. M.; Levent, M.; Ghosh, M.; Hoagland, S. M.; Varsolona, R. J.; Sutherland, K. A robust process for an mGluR5 negative allosteric modulator: Difluoromethylation and Sonogashira coupling on large scale. *Org. Process Res. Dev.* **2012**, *16*, 1854–1860.

(14) The TI denominator is defined as the species-specific total plasma concentration affording 80% mGlu5 RO over 24 h.

(15) Wager, T. T.; Hou, X.; Verhoest, P. R.; Villalobos, A. Moving beyond rules: The development of a central nervous system multiparameter optimization (CNS MPO) approach to enable alignment of druglike properties. *ACS Chem. Neurosci.* **2010**, *1*, 435–449.

(16) For a reference on ligand efficiency (LE), see: Hopkins, A. L.; Groom, C. R.; Alex, A. Ligand efficiency: A useful metric for lead selection. *Drug Discovery Today* **2004**, *9*, 430–431.

(17) For a reference on lipophilicity efficiency (LipE), see: Freeman-Cook, K.; Hoffman, R. L.; Johnson, T. W. Lipophilicity efficiency: The most important efficiency metric in medicinal chemistry. *Future Med. Chem.* **2013**, *5*, 113–115.

(18) Wager, T. T.; Chandrasekaran, R. Y.; Hou, X.; Troutman, M. D.; Verhoest, P. R.; Villalobos, A.; Will, Y. Defining desirable central nervous system drug space through the alignment of molecular properties, in vitro ADME and safety attributes. *ACS Chem. Neurosci.* **2010**, *1*, 420–434.

(19) RRCK cells were generated in-house (Pfizer Inc., Groton, CT, USA) as a subclone of Mardin-Darby canine kidney wild-type (MDCK-WT) cells that displayed low expression of endogenous P-gp (approximately 1 to 2% of MDCK-WT cells based on mRNA level). For detailed information, see: Callegari, E.; Malhotra, B.; Bungay, P. J.; Webster, R.; Fenner, K. S.; Kempshall, S.; LaPerle, J. L.; Michel, M. C.; Kay, G. G. A comprehensive non-clinical evaluation of the CNS penetration potential of antimuscarinic agents for the treatment of overactive bladder. *Br. J. Clin. Pharmacol.* **2011**, *72*, 235–246.

(20) Feng, B.; Mills, J. B.; Davidson, R. E.; Mireles, R. J.; Janiszewski, J. S.; Troutman, M. D.; de Morais, S. M. In vitro P-glycoprotein assays to predict the in vivo interactions of P-glycoprotein with drugs in the central nervous system. *Drug Metab. Dispos.* **2008**, *36*, 268–275.

(21) A dihedral torsional scan of the terminal pyridyl to the central pyrazolopyrazine using quantum mechanics indicates the lowest-energy dihedral angle of 0° for **12** and approximately 30° for **14**.

(22) Compound **14** was screened in two kinase selectivity panels: the Dundee panel (50 kinase targets) and the Invitrogen panel (40 kinase targets).

(23) The Pfizer in-house PDE selectivity panel consists of 11 PDE subtypes including PDE1b, PDE2a, PDE3a, PDE4d, PDE5a, PDE6a, PDE7b, PDE8b, PDE9a, PDE10a, and PDE11.

(24) BioPrint is a broad selectivity panel provided by CEREP consisting of 79 targets from different gene families.

(25) Lipinski, C. A.; Lombardo, F.; Dominy, B. W.; Feeney, P. J. Experimental and computational approaches to estimate solubility and permeability in drug discovery and development settings. *Adv. Drug Delivery Rev.* **2001**, *46*, 3–26.

(26) Hughes, J. D.; Blagg, J.; Price, D. A.; Bailey, S.; DeCrescenzo, G. A.; Devraj, R. V.; Ellsworth, E.; Fobian, Y. M.; Gibbs, M. E.; Gilles, R. W.; Greene, N.; Huang, E.; Krieger-Burke, T.; Loesel, J.; Wager, T. T.; Whiteley, L.; Zhang, Y. Physicochemical drug properties associated with in vivo toxicology outcomes. *Bioorg. Med. Chem. Lett.* **2008**, *18*, 4872–4875.

(27) The homology model was carried out with Prime 2.1 (Prime, version 2.1, Schrödinger, LLC, New York, NY, 2009). The A_{2A} adenosine receptor was used as template taking into account positions of highly conserved amino acid residues and known common motifs between class A and C G protein-coupled receptors. The default values of all prime parameters were used. The Glide 5.5 program (Glide, version 5.5, Schrödinger, LLC, New York, NY, 2009) was employed using the standard precision mode (SP) to generate the different binding poses of **14**. The receptor grid was generated on the basis of the eight amino acid residues identified by site-directed mutagenesis to affect MPEP affinity. Before the docking calculations, **14** and MPEP were submitted to an energy minimization using the OPLS_2005 force field and the GB/SA method as the implicit water model. To accommodate the fact that the protein structure used for docking will not, in general, be optimized to fit a particular ligand, the van der Waals radii for nonpolar protein atoms were scaled by a factor of 0.8, whereas those for the ligands were scaled to 1.0. The docking poses were selected by applying the MM-GB/SA method.

(28) Anderson, J. J.; Bradbury, M. J.; Giracello, D. R.; Chapman, D. F.; Holtz, G.; Roppe, J.; King, C.; Cosford, N. D. P.; Varney, M. A. In vivo receptor occupancy of mGluR5 receptor antagonists using the novel radioligand [³H]3-methoxy-5-(pyridin-2-ylethynyl)pyridine. *Eur. J. Pharmacol.* **2003**, *473*, 35–40.

(29) Using the unbound plasma **14** concentration ($C_{p,u}$) and observed RO for individual animals, both a direct-response model using a Hill equation and a receptor-binding kinetic model afforded an IC₅₀ of 1.04 nM and K_D of 0.49 nM, respectively. A 2-fold difference between IC₅₀ and K_D confirmed that the direct-response model was adequate and suggested that hysteresis because of slow binding kinetics is not anticipated. A profile likelihood 95% confidence interval was determined for the IC₅₀.

(30) A two-tissue (2T) compartment model was applied to fit the measured PET data in various brain regions to determine their volume of distribution (V_t). The mGlu5 RO was determined by analysis of

occupancy plots comparing the change in V_t in displacement scans relative to baseline V_t .

(31) Using the mean unbound plasma **14** concentration ($C_{p,u}$) over the scanning time period and the observed RO for each PET animal at a specific dose, a direct-response model using a Hill equation provided the IC₅₀ (0.43 nM). A profile likelihood 95% confidence interval was determined for the IC₅₀.

(32) Rylander, D.; Iderberg, H.; Li, Q.; Dekundy, A.; Zhang, J.; Li, H.; Baishen, R.; Danysz, W.; Bezar, E.; Cenci, M. A. An mGluR5 antagonist under clinical development improves L-DOPA-induced dyskinesia in parkinsonian rats and monkeys. *Neurobiol. Dis.* **2010**, *39*, 352–361.

(33) For details of the MPTP-rendered NHP PD-LID study design, see the Supporting Information.

(34) Palanisamy, G. S.; Marcek, J. M.; Cappon, G. D.; Whritenour, J.; Shaffer, C. L.; Brady, J. T.; Houle, C. Drug-induced cutaneous lesions in Cynomolgus macaques treated with metabotropic glutamate receptor 5 (mGluR5) negative allosteric modulators, 32nd Annual Symposium, Society of Toxicologic Pathology, Portland, OR, June 16–20, 2013; 88.

(35) Yang, W.; Choong, I. Azaindazoles as HCV replication inhibitors and their preparation, pharmaceutical compositions and use in the treatment of flaviviridae virus infection. WO 2011/049987, April 28, 2011.

(36) Cho, S.; Li, Q.; Ahn, S.; Bai, B.; Leahy, R. M. Iterative image reconstruction using inverse Fourier rebinning for fully 3-D PET. *IEEE Trans. Med. Imaging* **2007**, *26*, 745–756.

(37) Cunningham, V. J.; Rabiner, E. A.; Slifstein, M.; Laruelle, M.; Gunn, R. N. Measuring drug occupancy in the absence of a reference region: The Lassen plot re-visited. *J. Cereb. Blood Flow Metab.* **2010**, *30*, 46–50.